Arabian Journal of Geosciences (2018) 11: 717
https://doi.org/10.1007/s12517-018-4083-4

ORIGINAL PAPER

Chemical composition of rock-forming minerals and crystallization physicochemical conditions of the Middle Eocene I-type Haji Abad pluton, SW Buin-Zahra, Iran

Kazem Kazemi[1] · Ali Kananian[1] · Yilin Xiao[2] · Fatemeh Sarjoughian[3]

Received: 24 April 2018 / Accepted: 15 November 2018 / Published online: 23 November 2018

Abstract

The Haji Abad intrusion is a well-exposed Middle Eocene I-type granodioritc pluton in the Urumieh–Dokhtar magmatic assemblage (UDMA). The major constituents of the investigated rocks are K-feldspar, quartz, plagioclase, pyroxene, and minor Fe–Ti oxide and hornblende. The plagioclase compositions fall in the labradorite, andesine, and oligoclase fields. The amphiboles range in composition from magnesio-hornblende to tremolite–hornblende of the calcic-amphibole group. Most pyroxenes principally plot in the field of diopside. The calculated average pressure of emplacement is 1.9 kbar for the granodioritic rocks, crystallizing at depths of about 6.7 km. The highest pressure estimated from clinopyroxene geobarometry (5 kbar) reflects initial pyroxene crystallization pressure, indicating initial crystallization depth (17.5 km) in the Haji Abad granodiorite. The estimated temperatures using two-feldspar thermometry give an average 724 °C. The calculated average temperature for clinopyroxene crystallization is 1090 °C. The pyroxene temperatures are higher than the estimated temperature by feldspar thermometry, indicating that the pyroxene and feldspar temperatures represent the first and late stages of magmatic crystallization of Haji Abad granodiorite, respectively. Most pyroxenes plot above the line of $Fe^{3+} = 0$, indicating they crystallized under relatively high oxygen fugacity or oxidized conditions. Furthermore, the results show that the Middle Eocene granitoids crystallized from magmas with H_2O content about 3.2 wt%. The relatively high water content is consistent with the generation environment of HAG rocks in an active continental margin and has allowed the magma to reach shallower crustal levels. The MMEs with ellipsoidal and spherical shapes show igneous microgranular textures and chilled margins, probably indicating the presence of magma mixing. Besides, core to rim compositional oscillations (An and FeO) for the plagioclase crystals serve as robust evidence to support magma mixing. The studied amphiboles and pyroxenes are grouped in the subalkaline fields that are consistent with crystallization from I-type calc-alkaine magma in the subduction environment related to active continental margin. Mineral chemistry data indicate that Haji Abad granodiorites were generated in an orogenic belt related to the volcanic arc setting consistent with the subduction of Neo-Tethyan oceanic crust beneath the central Iranian microcontinent.

Keywords Thermobarometry · Mineral chemistry · Urumieh–Dokhtar magmatic arc · Haji Abad · Iran

Introduction

The Haji Abad intrusion is hosted within the Urumieh–Dokhtar magmatic assemblage (UDMA) as part of the Zagros orogeny (Fig. 1). Similar to other segments of the Alpine–Himalayan mountain chain, the Zagros orogeny formed as a consequence of closure of the Neo-Tethyan ocean and the continuing continental collision between Arabia and Eurasia (e.g., Berberian and Berberian 1981; Berberian and King 1981; Moine-Vaziri 1985; Arvin et al. 2007; Allen 2009) and is an outstanding natural laboratory for studying metamorphism and igneous rocks, continental orogenesis, and petrogenetic and geodynamic processes. Geologically, the Zagros

✉ Ali Kananian
kananian@khayam.ut.ac.ir

[1] School of Geology, College of Science, University of Tehran, Tehran, Iran

[2] Department of Geochemistry and Environmental Science, School of Earth and Space Sciences, University of Science and Technology of China, Hefei 230026, China

[3] Department of Earth Sciences, Faculty of Sciences, University of Kurdistan, Sanandaj, Iran

orogeny is made up of three NW–SE-trending parallel belts, which from north to south are the UDMA, Sanandaj–Sirjan structural zone (SSZ), and Zagros Fold–Thrust Belt (ZFTB) (Alavi 2004). UDMA which is 150 km wide is predominantly composed of tholeiitic, calc-alkaline, and K-rich alkaline intrusive and extrusive rocks with associated pyroclastic and volcanoclastic successions, and occurred along the active margin of the Iranian plate as an active continental magmatism (Alavi 2004). The intrusive rocks are dominantly composed of granite, granodiorite, and diorite that generally show calc-alkaline, metaluminous, I-type composition (e.g., Rezaei-Kahkhaei et al. 2011; Sarjoughian et al. 2012; Kananian et al. 2014; Kazemi et al. 2018). Though many studies have been done on the petrogenesis of these rocks, there are few studies conducted on mineral chemistry in order to determine the emplacement conditions and physicochemical parameters of the parental magma of these rocks.

The mineral assemblage and compositions in igneous rocks can be used to evaluate the physicochemical conditions of magma crystallization during the emplacement of intrusive rocks (e.g., Abbott 1985; Sarjoughian et al. 2015). So, the compositions and structures of the various mineral phases (feldspar, amphibole, pyroxene, etc) can serve as ideal proxies for the determination of magmatic processes and physicochemical parameters, such as pressure and temperature of crystallization, oxygen fugacity, H_2O contents, and composition of parental magma (Zhang et al. 2006; Honarmand et al. 2012; Murphy et al. 2012; Sepahi et al. 2012; Sherafat et al. 2012; Ayati et al. 2013; Sarjoughian et al. 2015). Many researchers proposed that using estimated crystallization pressure can readily determine the depths of emplacement and provide insights into the denudation history (e.g., Hammarstrom and Zen 1986; Vyhnal et al. 1991; Schmidt 1992; Anderson 1996; Stein and Dietl 2001; Zhang et al. 2006). The estimation of the emplacement depth during the solidification of calc-alkaline intrusions is an indicator of characterizing the complex chemical evolution and tectonic processes in orogenic belts, thus also provides indirect evidence for the ascent or descent of exposed crustal sections through time (Rutter et al. 1989; Tulloch and Challis 2000; Zhang et al. 2006).

Feldspar and pyroxene thermobarometry have been widely used to estimate the crystallization pressure and temperature of igneous rocks, providing tools to determine the emplacement depth of rocks (Helz 1973; Fuhrman and Lindsley 1988; Soesoo 1997; Putirka et al. 2003; Putirka 2005, 2008; Faak et al. 2013).

Amphibole-group minerals occur in a wide variety of igneous rocks formed in different tectonic environments and have an important influence in the subduction-related magmatic evolution (Anderson 1980; Ernst 1999; Davidson et al. 2007; Martin 2007; Larocque and Canil 2010; Ridolfi et al. 2010; Dessimoz et al. 2012; Krawczynski et al. 2012). Mafic magmas that are related to the subduction tectonic environment are usually hydrous, and the increase in water contents of such magmas induces the late-stage metasomatic processes and formation of interstitial amphibole (Claeson and Meurer 2004).

The Haji Abad intrusion is a well-exposed Middle Eocene I-type granodioritc pluton in the north of the Haji Abad village (Fig. 2) and contains abundant globular or elliptical mafic microgranular enclaves (MMEs) of various sizes, that provide an excellent case to investigate the physicochemical conditions in terms of many parameters accompanying magma emplacement and crystallization.

The Haji Abad pluton was intruded into the volcanosedimentary rocks (Fig. 2) that mainly consists of granodiorite and diorite along with aplitic dikes (Tabbakh Shabani 1991; Safarzadeh et al. 2007; Kazemi et al. 2018). This intrusive has been named granite in the geologic map of the Saveh quadrangle at 1:250,000 scale (Nogole-Sadat and Hoshmandzadeh 1984), but in the Danesfahan quadrangle map at 1:100,000 scale (Eghlimi 2000), it has been named as subvolcanic and plutonic rocks with diorite to granite suites. Kazemi et al. (2018) suggested that the Haji Abad granitoids are metaluminous, arc-related calc-alkaline, and I-type in composition. In addition, these researchers, based on field and petrographic characterization together with bulk rock geochemical and Nd–Sr isotopic data, suggested that host rocks and their MMEs originated by interaction between basaltic lower crust-derived felsic and mantle-derived mafic magmas in an active continental margin arc environment. The emplacement of the Haji Abad granitoid in the SW Buin-Zahra region took place ca. 40 Ma, representing an orogenic cycle in a preplate collision (Kazemi et al. 2018). Kazemi et al. (2018) concluded that the angle of subduction of Neo-Tethyan oceanic crust beneath central Iran is less than 15° for Eocene magmatism in the central UDMA interior, consistent with flat or low-angle subduction.

The in situ microanalysis of minerals (such as feldspar, amphibole, and pyroxene) is our approach to reinvestigate this intrusion where major element compositions are used for (1) estimations of crystallization temperature, pressure, oxygen fugacity, and H_2O content using mineral chemical compositions of Haji Abad granitoid (HAG) rocks; (2) determination of chemical composition, nature, and tectonic setting of their formative magma; and (3) exploration of petrogenetic processes, such as magma mixing, responsible for the formation of I-type intrusive rocks, using chemical zoning in the plagioclase crystals and petrography observations.

Geological setting and field relations

The HAG is located about 20 km southwestern of Buin-Zahra City in the central part of the UDMA within the structural zone of central Iran (Figs. 1 and 2).

The area is dominated by Eocene magmatic rocks that are the thickest and largest exposed unit (Fig. 2). The early Eocene volcanic rocks are the oldest geologic units in the study area and are traceable to the Oligocene, Miocene, Pliocene, and the Quaternary, that show facies variation from marine to continental eruptions.

The surrounding rocks in the Haji Abad intrusion are Eocene rhyodacitic tuff, dacitic pyroclastics, dacite-andesitic lava flows and breccia, basalt, andesitic basalt, dacitic ignimbrite, and tuffite (Fig. 2; Nogole-Sadat and Hoshmandzadeh 1984; Eghlimi 2000; Dorouzi and Vosoughi Abedini 2009).

Dacitic pyroclastics, mainly tuffs, are the oldest rocks, and they are mainly exposed in the southern and western parts of the Haji Abad granitoid and have the longest contact with the pluton. The northern and northeastern parts of the intrusion were emplaced into lower Eocene tuff, andesitic volcanics, and breccias, whereas the dacitic ignimberites are exposed in the south of the Haji Abad pluton. This pluton has a low height and hill morphology, while the surrounding volcanic rocks are higher.

These rocks are dominantly composed of olivine, plagioclase, clinopyroxene, amphibole, biotite, K-feldspar, and quartz. Geochemically, the basalt, andesitic basalt, andesite, and dacite belong to the subalkaline series and show calc-alkaline affinity. Based on their enrichment of LILE and LREE and relative depletion of HFSE, these rocks can be correlated with the subduction tectonic setting in an active continental margin (Dorouzi and Vosoughi Abedini 2009). The Oligocene starts with a clastic unit of conglomerate, sandstone, and marl of the Lower Red Formation followed by limestone marl and marl and finally changes to the periodicity of igneous and volcanoclastic units consisting of dacite, rhyolite, andesite, basalt, and ignimbrite. The younger geological units are marine and detrital sediments of Qom and Upper Red formations, which are deposited on top of the volcanic rocks during the Oligo-Miocene and Miocene, respectively.

Several plutonic bodies with K-Ar age of 39.2 ± 3.2 Ma (Caillat et al. 1978) in the vicinity of the Haji Abad granodiorite intruded the Eocene volcanosedimentary rocks that comprise gabbro, diorite, quart–diorite, quartz–monzodiorite, granodiorite, quartz–monzonite, and granite along with aplitic dikes (Tabbakh Shabani 1991; Kazemi et al. 2018) with transitional contact. The Haji Abad pluton forms a large SE–NW elongated body, elongated parallel to the regional faults; is medium-grained, granular, and light gray; and exposed over an area of > 40 km^2 that occurs at the intersection of the regional faults and shows weak contact metamorphism (Figs. 2 and 3a). This pluton comprises of granodiorite and minor diorite. The dioritic rocks scattered as small outcrops through the southern part of the area. These rocks are fine-grained and have a seriate texture with feldspar megacrysts along the margins that exhibit a chilled margin, but toward the center, gradually change to a granular texture. The study of Kazemi et al. (2018) revealed that the Haji Abad granitoids are medium- to high-K calc-alkaline, metaluminous, magnetite series and I-type igneous rocks.

It is notable that microgranular enclaves of various sizes are common throughout the Haji Abad granodiorites (Fig. 3b). They are globular or elliptical in shape, 2–30 cm in diameter, and display hypidiomorphic microgranular texture and sharp boundaries with their hosts. These enclaves are fine-grained and darker than their host rocks and comprised of diorite and gabbro-diorite. They are structurally massive with chilled margins toward the enclave rims.

Analytical methods

Electron probe microanalyses (EPMA) of mineral assemblages were carried out using a JEOL JXA-8230 Superprobe at Hefei University, China. The operating conditions were 15 kV accelerating voltage, 10 nA (K-feldspar and plagioclase) and 20 nA (amphibole and pyroxene) beam current, and 5 μm beam diameter. Structural formulae calculations of feldspars are based on eight atoms of oxygen. Structural formulae of amphibole are calculated on the basis of 23 oxygens. Pyroxenes are classified by using the total numbers of specified cations at the M sites based on the six oxygen atoms.

Field and petrography observation

The predominant intrusive rock of the investigated area is granodiorites that are gray and massive, and the diorites are scattered as separate and small outcrops throughout the southern part of the area and are fine-grained and seriate with feldspar megacrysts along the margins, but they increase in grain size and become granular toward the center. The major constituents of the investigated rocks are K-feldspar, quartz, plagioclase, pyroxene, and minor Fe–Ti oxide, and hornblende (Fig. 3c–f), and the accessory minerals (< 1%) include euhedral to rounded zircon, prismatic to acicular apatite, and titanite. Plagioclase occurs as euhedral to anhedral crystals, zoned and altered to sericite, epidote, and calcite, whereas the K-feldspars occur as anhedral grains. Plagioclase with sieve-textured and poikilitic texture (Fig. 3c, e) are the common features in these samples. Some plagioclase crystals show rounding and corroded margins. Marginal comminution and the rounded corners of plagioclase grains can be an indicator of magma mixing (e.g., Zorpi et al. 1989; Shelley 1993). Pyroxene as euhedral to subhedral crystals is a dominant mafic phase in all the rocks of the HAG. Pyroxene crystals are partly to completely

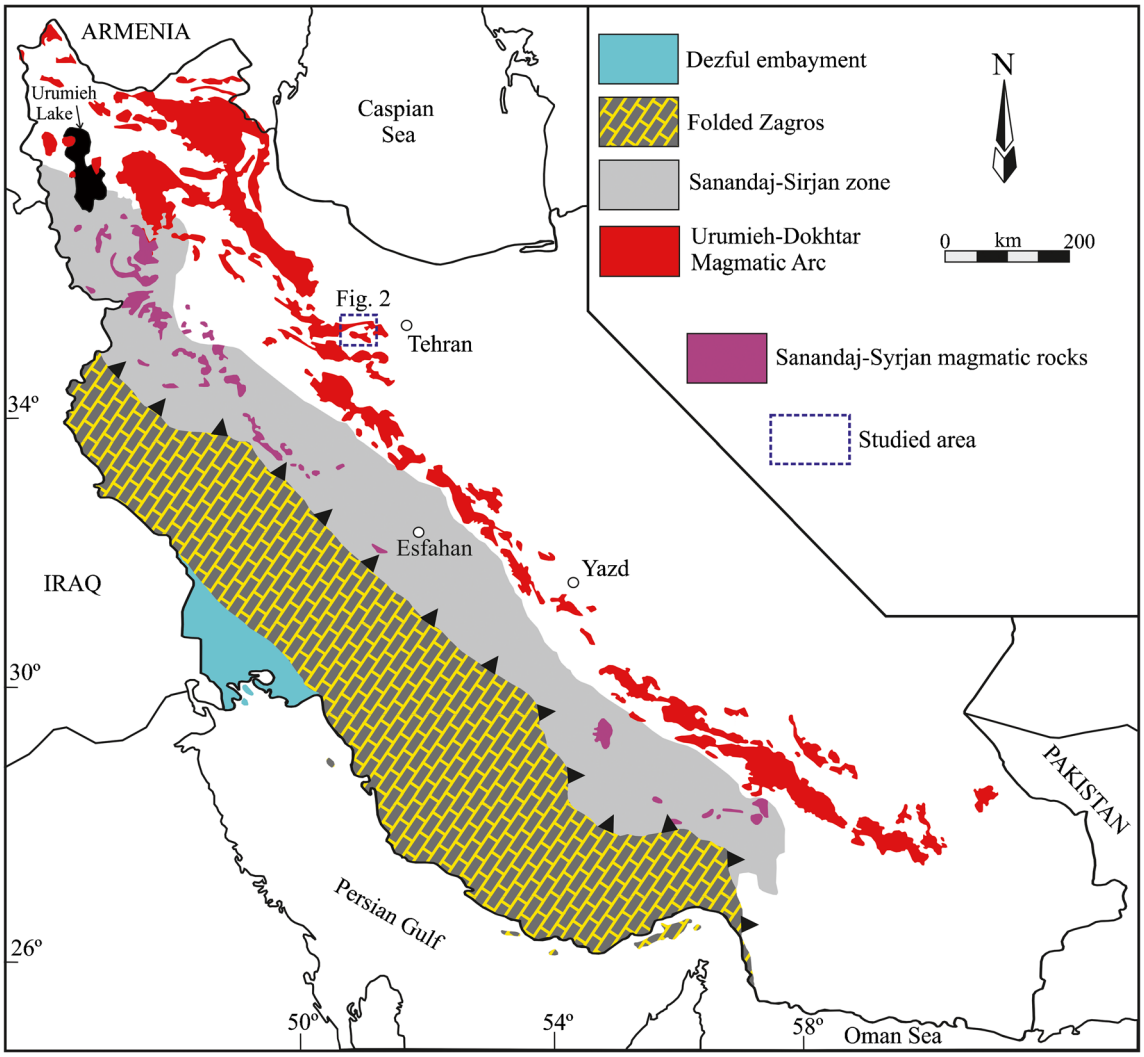

Fig. 1 Simplified geology of the western Iran showing the Sanandaj–Sirjan zone (SSZ), main Zagros thrust (MZT), and Urumieh–Dokhtar magmatic arc (UDMA) (modified after Aghanabati 1998)

transformed to actinolite as a result of hydrothermal alteration (Fig. 3c). Hornblende is commonly at interstitial phase and is rarely altered to tremolite hornblende, chlorite, and titanite. Quartz forms anhedral crystals or aggregates of several grains with irregular boundaries (Fig. 3e).

MME comprises mafic mineral assemblages, relatively fine-grained and commonly globular to ellipsoidal shaped having a typical igneous microstructure (e.g., Vernon 1990; Barbarin 2005) with various sizes (Fig. 3b). These enclaves are present throughout the intrusion and are characterized by a hypidiomorphic microgranular texture and are structurally massive (Fig. 3f). The majority of the enclaves have chilled margins and sharp boundaries with their host granodiorite, although some MMEs have transitional contacts with their host rock. The MMEs mainly comprise of pyroxene, plagioclase, K-feldspar, quartz, and hornblende (Fig. 3f). The plagioclases occur as euhedral–subhedral tabular-prismatic shape. The pyroxenes are the most abundant dark mineral, followed by amphiboles.

Mineral chemistry

Feldspar

The results of EPMA analysis of plagioclases and K-feldspar from the Haji Abad granodiorite are presented in Table 1 and are shown in a Ab–An–Or ternary diagram (Fig. 4). The compositions of K-feldspar crystals vary from Or_{77} to Or_{95}. The anorthite contents of plagioclases in the rocks range 9.8–60.2 mol%, and in the Ab–An–Or diagram (Deer et al. 1992), all of them plot mainly in the labradorite, andesine, and oligoclase fields (Fig. 4). Plagioclase crystals commonly show oscillatory zoning (Fig. 5). The core to rim

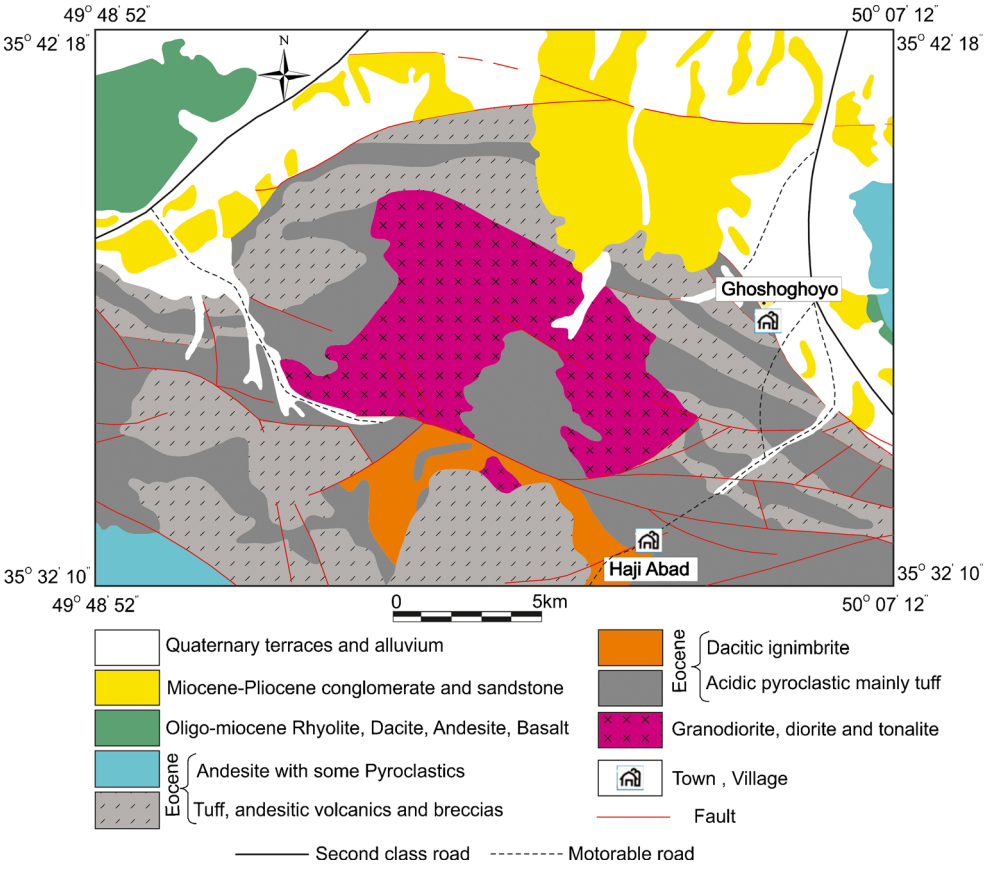

Fig. 2 Geological map of the Haji Abad granitoid. Simplified and modified from 1:250,000 Saveh map by Nogole-Sadat and Hoshmandzadeh (1984)

EPMA analyses of three plagioclases, HG45-1-P, HG45-2-P, and HG45-4-P, all show oscillatory variations of An values from the center to the rime.

Pyroxene

The results of 25 point analyses performed on 15 representative clinopyroxene crystals from HAG are presented in Table 2 and are plotted in the diagram of Wo–En–Fs (Fig. 6a). In the Wo–En–Fs diagram of Morimoto et al. (1988), most of them principally plot in the field of diopside and some in the augite field (Fig. 6a). They are classified as the "Quad" or Ca–Mg–Fe clinopyroxenes (Fig. 6b; Morimoto et al. 1989). Clinopyroxenes are rich in Ca ($Wo_{46.67}$) but poor in Na ($Na_2O < 0.44$). Their compositions range from $En_{38}Fs_9Wo_{43}$ to $En_{44}Fs_{15}Wo_{49}$.

Amphibole

The results of EPMA analysis of amphibole samples from the Haji Abad granodiorite are presented in Table 3 and plotted on the BCa+BNa versus BNa diagram (Leake et al. 1997) (Fig. 7a). They range in composition from magnesio-hornblende to hornblende and to tremolite–hornblende of the calcic-amphibole group [calculated Ca_B (B-site; apfu—atoms per formula unit) is higher than 1.50 apfu, Ca_A is lower than 0.5 apfu, the $(Na+K)_A$ (A-site) is lower than 0.5 apfu] following the nomenclature of Leake et al. (1997) (Fig. 7b). The chemical composition of amphibole in the HAG has wide Al_2O_3 and SiO_2 ranges from 2.87 to 4.16 wt% and from 49.57 to 53.1 wt%, respectively, while their Mg# (Mg/(Mg+Fe)) varies between 0.88 and 0.96 (Table 3).

Discussion

Estimation of pressure, temperature, oxygen fugacity, and water contents

Compositions of the mineral chemistry are used to determine the physicochemical crystallization conditions such as temperature, pressure, H_2O contents, and oxygen fugacity. The estimations of crystallization temperature, pressure, H_2O content, and oxygen fugacity using feldspar and pyroxene minerals of granitoid rocks were proposed by some researchers such as Helz (1973), Fuhrman and Lindsley (1988), Soesoo (1997), Putirka et al. (2003), Putirka (2005, 2008), and Faak et al. (2013).

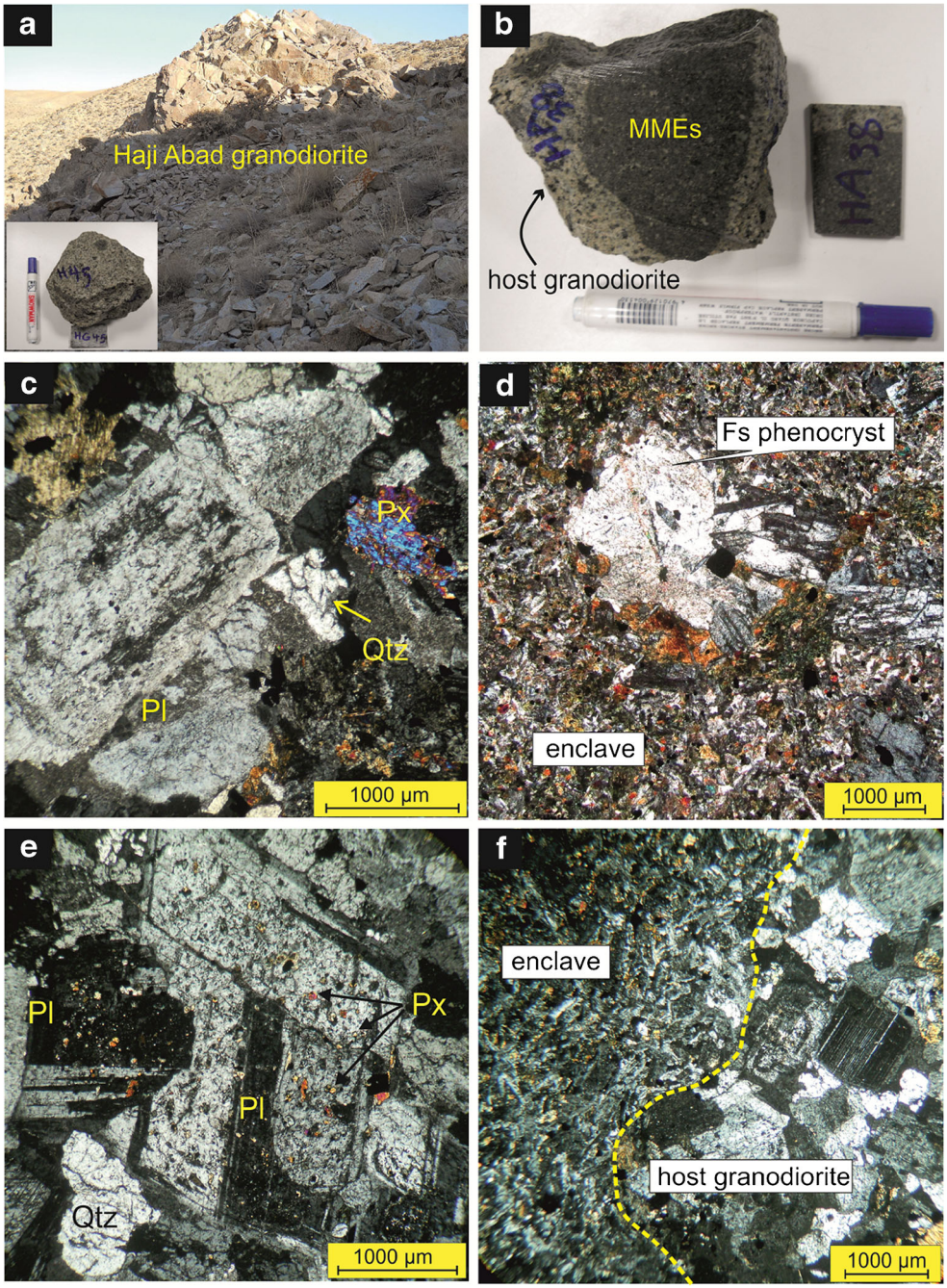

Fig. 3 Field photograph and thin section representative microphotographs (cross-polarized light) of the Haji Abad granitoids and their enclaves: **a** field photograph showing the Haji Abad granodiorite, **b** microgranular enclaves hosted by granodiorite, **c** granodiorite with granular texture including sieved plagioclase, **d** feldspar phenocrysts hosted by microgranular enclave, **e** poikilitic texture and resorption surface in the granodiorite, and **f** photomicrograph showing the relationship between microgranular enclave and host granodiorite. Abbreviations: Pl, plagioclase; Px, pyroxene; Qtz, quartz. Mineral abbreviations are from Kretz (1983)

Pressure and temperature conditions of crystallization

The plagioclase and pyroxene compositions are sensitive to variations in the chemistry of magma and the pressure and temperature crystallization conditions. The pyroxene crystallization pressures obtained from granodiorite using the X_{PT} and Y_{PT} parameters are shown in Fig. 8a (Soesoo 1997). X_{PT} and Y_{PT} parameters were calculated using the following methods:

$$X_{PT} = 0.446SiO_2 + 0.l87TiO_2 - 0.404A1_2O_3 + 0.346FeO^{tot} - 0.052MnO + 0.309MgO + 0.431CaO - 0.446Na_2O$$

$$Y_{PT} = -0.369SiO_2 + 0.535TiO_2 - 0.317A1_2O_3 + 0.323FeO^{tot} + 0.235MnO - 0.5l6MgO - 0.167CaO - 0.l53Na_2O$$

Table 1 Representative electron microprobe analyses (wt%) of feldspar minerals of the Haji Abad granodiorites

Lithology	Granodiorite	Granodiorite	Granodiorite	Granodiorite	Granodiorite	Granodiorite	Granodiorite	Granodiorite	Granodiorite	Granodiorite	Granodiorite	Granodiorite	Granodiorite
Sample	HG45-1-PR	HG45-1-PM1	HG45-1-PM2	HG45-1-PM3	HG45-1-PC	HG45-1-P21	HG45-1-P22	HG45-2-PR	HG45-2-PM1	HG45-2-PM2	HG45-2-PM3	HG45-2-PM4	HG45-2-PC
SiO_2	63.65	54.95	53.74	57.68	65.38	63.83	56.22	63.66	57.34	53.87	58.32	57.79	57.16
TiO_2				0.021	0.018	0.056				0.013		0.067	
Al_2O_3	21.50	27.15	28.38	25.57	20.40	20.91	26.44	21.87	25.40	28.14	24.60	24.69	25.86
FeO	0.14	0.38	0.40	0.24	0.15	0.20	0.28	0.12	0.30	0.27	0.28	0.34	0.25
MnO			0.063	0.010	0.053	0.029	0.044		0.024			0.010	
MgO		0.035	0.051	0.005		0.004			0.005	0.034	0.003		0.023
CaO	3.79	11.58	12.86	8.88	2.11	3.19	10.29	4.05	8.93	12.29	8.28	8.46	9.49
Na_2O	8.70	5.37	4.54	6.71	10.02	9.42	5.79	9.14	6.63	4.99	6.85	6.88	6.20
K_2O	0.77	0.26	0.21	0.32	0.97	0.66	0.23	0.63	0.46	0.26	0.52	0.53	0.42
BaO		0.001	0.009		0.017			0.014	0.001	0.019			
Total	98.63	99.73	100.34	99.51	99.19	98.55	99.57	99.57	99.10	99.91	99.16	98.76	99.70
Ab (%)	77.0	45.0	38.5	56.7	84.7	81.1	49.8	77.5	55.9	41.7	58.2	57.8	52.9
An (%)	18.5	53.6	60.3	41.5	9.9	15.2	48.9	19.0	41.6	56.8	38.9	39.2	44.8
Or (%)	4.5	1.4	1.2	1.8	5.4	3.7	1.3	3.5	2.6	1.4	2.9	2.9	2.4
Sample	HG45-3-P1	HG45-3-P21	HG45-3-P22	HG45-4-P1R	HG45-4-PM1	HG45-4-PM2	HG45-4-PM3	HG45-4-PC	HG45-4-P2R	HG45-4-P2M1	HG45-4-P2M3	HG45-4-P2C	HG45-5-P1
SiO_2	63.16	61.29	58.20	61.22	58.12	56.71	59.07	57.07	61.44	58.17	58.20	54.94	62.29
TiO_2				0.01	0.04								
Al_2O_3	22.25	23.32	24.34	23.23	25.51	26.08	24.58	25.68	23.46	24.93	24.92	27.03	22.04
FeO	0.17	0.22	0.28	0.17	0.31	0.30	0.33	0.21	0.16	0.23	0.33	0.28	0.17
MnO	0.039	0.05	0.03		0.02	0.01	0.02	0.04		0.05		0.01	0.11
MgO			0.01		0.03	0.01	0.02	0.01	0.03	0.03	0.03	0.06	
CaO	4.33	6.16	7.87	6.20	8.87	9.68	8.10	9.46	6.14	8.12	8.33	10.40	5.18
Na_2O	8.81	7.80	6.79	7.74	6.59	6.05	6.82	6.50	8.13	6.82	6.70	5.56	8.44
K_2O	0.60	0.45	0.53	0.42	0.41	0.39	0.53	0.31	0.55	0.59	0.57	0.37	0.56
BaO	0.009		0.02		0.01		0.01	0.02		0.03			
Total	99.36	99.33	98.43	99.00	99.93	99.45	99.56	99.30	99.90	98.96	99.44	98.75	98.86
Ab (%)	75.9	67.83	59.11	67.67	56.04	51.90	58.56	54.47	68.40	58.34	57.39	48.14	72.32
An (%)	20.6	29.62	37.83	29.93	41.67	45.91	38.43	43.81	28.55	38.37	39.41	49.73	24.53
Or (%)	3.4	2.6	3.1	2.4	2.3	2.2	3.0	1.7	3.1	3.3	3.2	2.1	3.2
Sample	HG45-8-P11	HG45-8-P12	HG45-4-P2M2	HG45-7-P	HG45-5-F1R	HG45-5-F1M1	HG45-5-F1M2	HG45-5-F1M3	HG45-5-F1C	HG45-5-F2R	HG45-5-F2M1	HG45-5-F2M2	HG45-5-F2M3
SiO_2	58.07	63.42	58.39	64.12	64.97	63.42	65.20	65.88	65.17	65.18	65.03	64.78	64.63
TiO_2	0.02		0.02			0.03	0.06						0.00
Al_2O_3	24.82	21.44	25.22	21.56	17.91	17.71	17.70	18.10	18.04	17.96	17.90	17.76	17.94
FeO	0.35	0.16	0.33	0.19	0.08	0.03	0.02	0.15	0.09	0.06	0.08	0.08	0.11
MnO	0.11	0.07		0.08		0.01			0.01			0.10	0.06
MgO	0.00	0.01	0.02	0.02				0.01					
CaO	8.46	4.10	8.92	3.82	0.11		0.11	0.11	0.05	0.15	0.03	0.04	0.04
Na_2O	6.90	9.30	6.95	9.14	1.46	0.71	2.50	1.89	1.33	1.99	1.74	1.85	1.64
K_2O	0.45	0.68	0.46	0.70	14.59	15.96	13.22	14.26	14.67	14.10	14.45	14.15	14.53
BaO	0.02	0.02									0.02		
Total	99.35	99.35	100.31	99.74	99.38	98.73	99.30	100.39	99.44	99.43	99.36	98.86	99.18
Ab (%)	58.11	77.42	57.06	78.07	13.13	6.32	22.19	16.70	12.07	17.56	15.46	16.53	14.61
An (%)	39.38	18.87	40.46	18.02	0.56	0.00	0.53	0.54	0.24	0.72	0.13	0.18	0.20
Or (%)	2.5	3.7	2.5	3.9	86.3	93.7	77.3	82.8	87.7	81.7	84.4	83.3	85.2
Sample	HG45-5-F2C		HG45-5-F31	HG45-7-F1		HG45-7-F2	HG45-8-F11		HG45-8-F12	HG45-8-F21		HG45–8-F22	
SiO_2	64.41		64.62	65.16		65.62	65.29		63.42	65.32		65.15	
TiO_2						0.07						0.04	
Al_2O_3	18.19		18.15	18.05		18.01	18.07		18.00	18.02		17.81	
FeO	0.07		0.07	0.17		0.06	0.11		0.01	0.05		0.06	
MnO	0.04		0.03			0.06	0.05			0.08			
MgO													
CaO	0.18			0.09		0.10	0.09		0.04	0.10		0.03	
Na_2O	1.98		0.54	1.51		1.83	2.21		0.66	1.75		0.65	
K_2O	13.38		16.39	15.10		14.05	13.88		15.99	14.38		16.24	

Table 1 (continued)

Lithology	Granodiorite	Granodiorite	Granodiorite	Granodiorite	Granodiorite	Granodiorite	Granodiorite	Granodiorite	Granodiorite	Granodiorite	Granodiorite
BaO		0.02		0.00	0.01		0.03				
Total	98.55	100.08	100.12	100.04	99.75		98.21	99.74		99.99	
Ab (%)	18.23	4.79	13.14	16.42	19.39		5.91	15.49		5.71	
An (%)	0.91	0.00	0.41	0.48	0.42		0.21	0.51		0.15	
Or (%)	80.9	95.2	86.4	83.1	80.2		93.9	84.0		94.1	

Ab, albite; *An*, anorthite; *Or*, orthoclase

The results illustrate clearly that all the pyroxenes fall within the < 2-kbar pressure.

Putirka (2008) proposed a geobarometry base on clinopyroxene compositions that can be used in granitic rocks. According to the proposed barometers (equations 30 and 32c: Putirka 2008), the averages of calculated pressures are 1.9 and 1.8 kbar, respectively. The highest calculated pressure using the clinopyroxene geobarometry is 5 kbar, which reflects initial pyroxene crystallization pressure, indicating initial crystallization depth (17.5 km) in the Haji Abad granodiorite.

Assuming that 1 kbar is comparable to ca. 3.5 km of the crust, they were emplaced at ca. 6.6 km in depth. Petrographic and textural pieces of evidence such as medium- to fine-grained and sharp angular contacts to the uppermost crustal country rocks where low-grade metamorphic aureole, hydrothermal alteration, and cognate volcanic rocks nearby were exposed suggest high-level emplacements in the granodiorite rocks that are in good agreement with the abovementioned results (Clarke 1992). The calculated pressure (1.9 kbar) for the HAG is compatible with suggested thicknesses (ca. 3–9 km) of Paleogene volcanic and sedimentary rocks in the Urumieh–Dokhtar magmatic assemblage (e.g., Förster et al. 1972; Morley et al. 2009). Moreover, the estimated pressures from the other plutonic rocks in UDMA, such as lower Eocene Kuh-e Dom pluton (1.3 kbar; Sarjoughian et al. 2012), Natanz pluton (2.1–2.5 kbar; Honarmand et al. 2012), Oligo-Miocene Nabar pluton (2–2.15 kbar; Abbasi et al. 2014), and Miocene Niyasar plutonic complex (0.2–1.7 kbar; Honarmand et al. 2016), are in good agreement with the pressure of HAG, indicating that most of the Paleogene granitoids in the UDMA intruded into the Eocene volcanic rocks. The mentioned discussions suggest that these shallow intrusions formed under overburden pressures of < 3 kbar.

Several models of two- and three-feldspar thermometry have been proposed (e.g., Nekvasil and Burnham 1987; Fuhrman and Lindsley 1988; Elkins and Grove 1990). The estimated temperatures using ternary-feldspar thermometry (Fuhrman and Lindsley 1988) range from 518 to 649 °C, with average 585 ± 40 °C. But it should be noted that this thermometry probably displays the subsolidus temperature that is lower than the actual feldspar crystallization temperature.

Two-feldspar thermometry (Putirka 2008: Eq. 27a) is the other thermometry that we use for the estimation of crystallization temperature. This thermometry shows relatively higher temperature than the previous geothermometer, with an average value of 724 ± 23 °C.

Plagioclase and pyroxene are commonly coexisting minerals in igneous rocks in a wide range of temperature and compositions and are used for geothermometry (Faak et al. 2013). Clinopyroxene–plagioclase thermometry was developed by Faak et al. (2013) based on experiments in the temperature-sensitive exchange of Mg between clinopyroxene

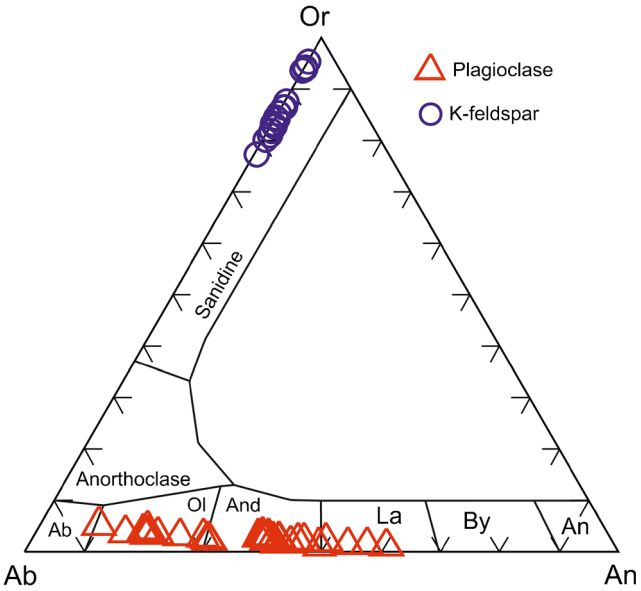

Fig. 4 Compositions of feldspars of the Haji Abad pluton on the Ab–An–Or diagram (Deer et al. 1992). Or, potassium feldspar; Ab, albite; Ol, oligoclase; And, andesine; La, labradorite; By, bytownite; An, anorthite

and plagioclase, according for different anorthite contents in plagioclase (X_{An}) and various silica activities (a_{SiO2}) in the system:

$$T[\mathrm{K}] = (-9219 + 2034X_{An})/\left(\ln K_{Mg}^{Pl/Cpx} - 1.6 - \ln a_{SiO2}\right).$$

Using this geothermometry, the calculated temperatures range from 633 to 822 °C (with an average of 741 ± 20 °C). The estimated temperature corresponds well with the two-feldspar thermometry results.

Furthermore, we used the X_{PT} versus Y_{PT} diagram of Soesoo (1997) for determination of the pyroxene crystallization temperature (Fig. 8b). It suggests that the pyroxenes crystallized under the temperature of 1150–1200 °C. Likewise, two methods from Putirka (2008) (equations 32d and 34) are used for the estimation of temperature conditions of clinopyroxene crystallization. According to equations 32d and 34, the calculated temperatures for clinopyroxene crystallization range from 1009 to 1144 °C (with an average of 1090 °C) and 947 to 1171 °C (with an average of 1014 °C), respectively. These temperatures are higher than the estimated temperature by feldspar thermometry, indicating that the pyroxene and feldspar temperatures represent the first and late stages of magmatic crystallization of Haji Abad granodiorite, respectively.

Oxygen fugacity (fO_2), H_2O contents, and density

Oxygen fugacity has an important influence on the liquidus temperature, melt and crystal composition, magmatic process control, crystallization sequence, and types of crystallized minerals (Botcharnikov et al. 2005; France et al. 2010). Schweitzer et al. (1979) suggested that the Fe^{3+} content of

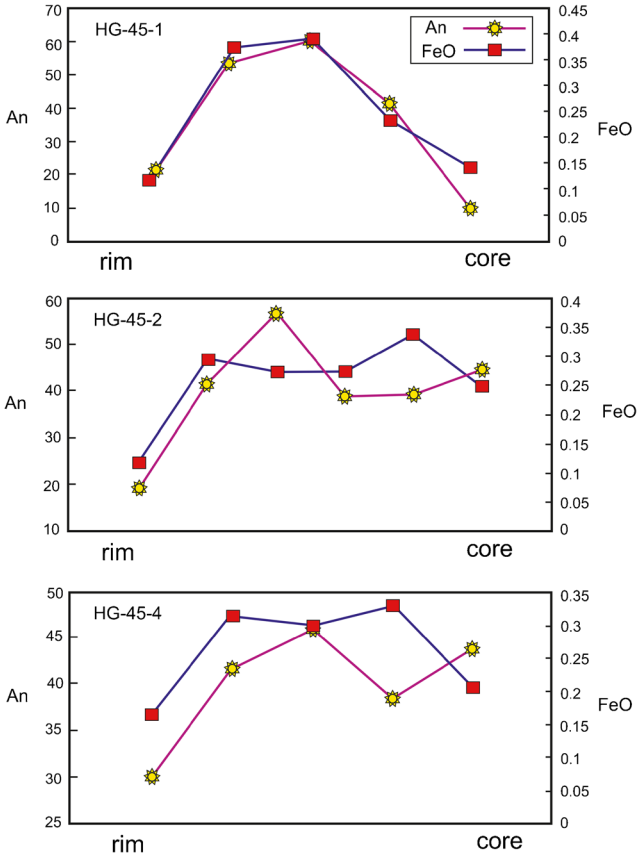

Fig. 5 Measured EPMA profiles for representative plagioclase crystals from the Haji Abad granodiorite, indicating oscillatory zoning

the pyroxenes depends on the oxygen fugacity of their generation environment, and is shown on the Al^{IV}+Na versus Al^{VI}+2Ti+Cr plot. Papike and Cameron (1976) have mentioned distances of the plotted samples from the line of Fe^{3+} and suggested that the more distance of samples from the line is indicative of a higher amount of oxygen fugacity in their formation environment. When the samples of granodiorite are plotted on the diagram, most of them plot above the line of $Fe^{3+} = 0$, indicating that they crystallized under relatively high oxygen fugacity or oxidized conditions (Fig. 8c).

The water contents have a considerable influence on plagioclase-melt equilibria (e.g., Kudo and Weill 1970; Housh and Luhr 1991; Panjasawatwong et al. 1995). Putirka (2005) proposed a hygrometric formulation for the calculation of water contents based on plagioclase-melt compositions. According to the plagioclase-melt hydrometer of Putirka (2005), the average of water contents in the Haji Abad granodiorite is about 3.2 wt%. The calculated water content is consistent with the generation environment of HAG rocks in an active continental margin and has allowed the magma to reach shallower crustal levels.

Because of released water from the subducted oceanic slab and its transfer to a higher level and eventually the role of released fluids in the production of magma, this leads to the

Table 2 Representative electron microprobe analyses (wt%) and structural formulae (cpfu) of pyroxene of the Haji Abad granitoids

Sample	HG45-1-PX1	HG45-1-PX2	HG45-3-PX1	HG45-3-PX2	HG45-4-P1R	HG45-4-P1C	HG45-4-P2R	HG45-4-P2C	HG45-6-PX11	HG45-6-PX12	HG45-6-PX2R	HG45-6-PX2C	HG45-6-PX31
SiO_2	53.84	53.79	53.28	53.94	54.16	54.14	54.07	53.22	53.87	53.64	53.41	54.12	53.46
TiO_2	0.00	0.08	0.13	0.02		0.06	0.05	0.13	0.04		0.01	0.04	0.04
Al_2O_3	0.45	0.24	0.67	0.32	0.21	0.33	0.27	0.79	0.34	0.21	0.45	0.35	0.35
FeO	7.14	6.50	7.61	7.74	6.50	6.96	6.61	7.86	6.74	7.13	8.94	6.47	7.28
MgO	14.97	14.77	14.43	14.90	15.13	14.98	15.03	14.41	15.01	14.77	14.02	15.47	15.21
CaO	22.82	23.93	22.69	22.76	23.42	23.28	23.47	22.50	22.85	23.75	22.17	23.30	22.78
Na_2O	0.34	0.29	0.35	0.31	0.35	0.32	0.29	0.39	0.24	0.24	0.26	0.33	0.27
K_2O	0.01	0.01		0.01	0.02		0.01				0.00		
Total	99.59	99.62	99.15	100.09	99.80	100.08	99.84	99.30	99.09	99.73	99.25	100.08	99.39
Si	1.998	1.996	1.991	1.998	2.002	2.000	2.001	1.986	2.009	1.991	2.005	1.993	1.987
Ti	0.000	0.002	0.004	0.001	0.000	0.002	0.001	0.004	0.001	0.000	0.000	0.001	0.001
Al^{IV}	0.002	0.002	0.005	0.002				0.010		0.009		0.006	0.012
Al^{VI}	0.018	0.009	0.024	0.012	0.011	0.016	0.014	0.025	0.025	0.000	0.025	0.009	0.004
Fe^{3+}	0.008	0.014	0.006	0.012	0.013	0.006	0.004	0.014	0.000	0.026	0.000	0.021	0.027
Fe^{2+}	0.213	0.188	0.232	0.227	0.188	0.209	0.201	0.232	0.210	0.195	0.281	0.178	0.199
Mg	0.828	0.817	0.804	0.822	0.834	0.825	0.829	0.802	0.835	0.817	0.785	0.849	0.843
Ca	0.907	0.952	0.909	0.903	0.928	0.921	0.931	0.900	0.913	0.944	0.891	0.919	0.907
Na	0.024	0.021	0.025	0.022	0.025	0.023	0.021	0.028	0.017	0.017	0.019	0.023	0.019
K	0.000	0.000	0.000	0.000	0.001	0.000	0.000	0.000	0.000	0.000	0.000	0.000	0.000
Sum cation	4.000	4.000	4.000	4.000	4.000	4.000	4.000	4.000	4.000	4.000	4.000	4.000	4.000
$Mg/(Mg+Fe^{2+})$	0.795	0.813	0.776	0.783	0.816	0.798	0.805	0.776	0.786	0.807	0.729	0.827	0.809
Wo	47	49	47	46	48	47	47	47	46	48	45	47	47
En	42.502	41.756	41.346	42.115	42.771	42.189	42.303	41.467	42.257	41.767	39.882	43.627	43.249
Fs	10.933	9.606	11.944	11.639	9.654	10.683	10.228	11.985	11.512	9.967	14.806	9.151	10.205
Sample	HG45-6-PX11	HG45-6-PX12	HG45-6-PX21	HG45-6-PX22	HG45-6-PX31	HG45-6-PX32	HG45-8-PX11	HG45-8-PX12	HG45-8-PX21	HG45-8-PX22	HG45-8-PX31	HG45-8-PX32	
SiO_2	53.32	54.21	53.54	52.71	53.95	52.99	53.10	53.40	53.28	53.55	54.04	53.73	
TiO_2	0.11	0.07	0.06	0.07	0.06	0.07	0.07	0.01	0.08	0.02		0.07	
Al_2O_3	0.48	0.32	0.56	0.94	0.26	0.68	0.27	0.17	0.66	0.40	0.25	0.33	
FeO	9.09	7.98	7.86	7.72	6.94	7.39	8.52	8.09	8.74	9.39	6.18	7.10	
MgO	14.02	14.81	15.03	14.39	15.24	14.46	15.09	14.80	13.50	13.38	15.08	14.73	
CaO	22.85	22.35	22.27	21.88	22.49	22.75	21.30	22.56	23.17	23.15	24.06	23.14	
Na_2O	0.30	0.31	0.36	0.41	0.29	0.32	0.23	0.16	0.44	0.32	0.21	0.29	
K_2O													
Total	100.17	100.09	99.71	98.11	99.24	98.65	98.58	99.22	99.88	100.21	99.83	99.39	
Si	1.984	2.009	1.987	1.989	2.008	1.989	1.997	1.998	1.987	1.997	1.998	2.001	
Ti	0.003	0.002	0.002	0.002	0.002	0.002	0.002	0.000	0.002	0.001	0.000	0.002	
Al^{IV}	0.013	−0.011	0.011	0.009	−0.010	0.009	0.001	0.002	0.010	0.002	0.002	−0.002	
Al^{VI}	0.008	0.025	0.013	0.033	0.021	0.021	0.011	0.006	0.019	0.015	0.009	0.017	
Fe^{3+}	0.027	0.000	0.024	0.006	0.000	0.012	0.006	0.007	0.024	0.010	0.007	0.002	
Fe^{2+}	0.256	0.247	0.220	0.238	0.216	0.220	0.262	0.246	0.249	0.283	0.184	0.220	
Mg	0.778	0.818	0.832	0.809	0.845	0.809	0.846	0.825	0.751	0.744	0.831	0.818	
Ca	0.911	0.887	0.885	0.885	0.897	0.915	0.858	0.904	0.926	0.925	0.953	0.923	
Na	0.021	0.022	0.026	0.030	0.021	0.024	0.017	0.011	0.032	0.023	0.015	0.021	
K	0.000	0.000	0.000	0.000	0.000	0.000	0.000	0.000	0.000	0.000	0.000	0.000	
Sum cation	4.000	4.000	4.000	4.000	4.000	4.000	4.000	4.000	4.000	4.000	4.000	4.000	
$Mg/(Mg+Fe^{2+})$	0.752	0.758	0.791	0.773	0.789	0.786	0.764	0.770	0.751	0.724	0.819	0.788	
Wo	47	45	45.718	45.792	45.566	47.063	43.655	45.781	48	47	48	47	
En	40.003	41.610	42.945	41.897	42.944	41.615	43.028	41.774	38.992	38.108	42.239	41.713	
Fs	13.157	13.262	11.337	12.311	11.490	11.323	13.317	12.444	12.925	14.497	9.329	11.202	

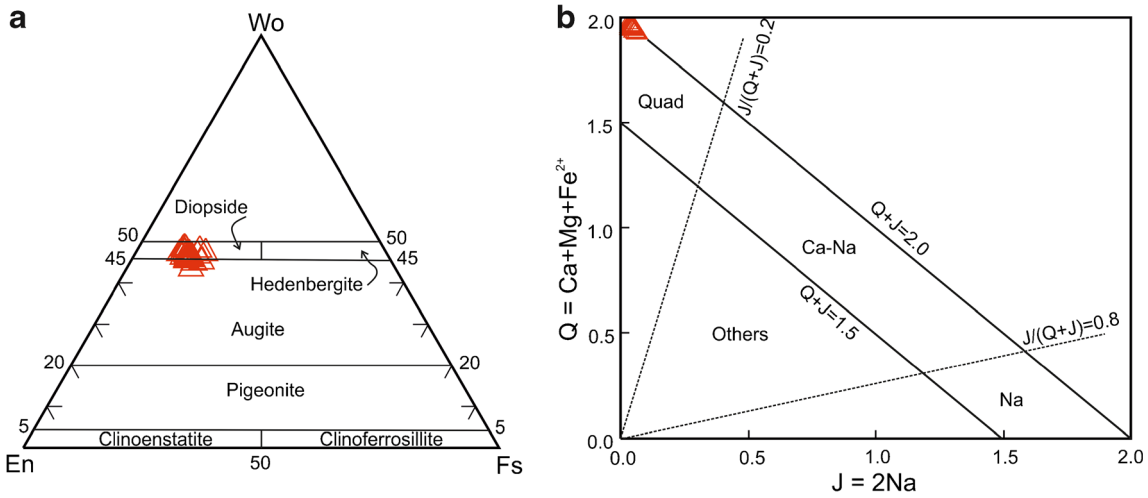

Fig. 6 **a** En–Wo–Fs ternary (Morimoto et al. 1988) and **b** Q=Ca+Mg+Fe^{2+} versus J=2Na diagrams (Morimoto et al. 1989) for the determination of clinopyroxene compositions

hydration of igneous rocks in the subduction zone environment (Sarjoughian 2012).

The abovementioned pieces of evidence indicate that the Haji Abad intrusion had probably been saturated with water before the final solidification. H_2O is the main volatile phase dissolved in natural aluminosilicate melts and strongly affects the physicochemical attributes of melts such as phase relationships, viscosity, density, and diffusivity. Therefore, dissolved water can control magma's ability to separate from the source and melt crystallization (Snelling and Woodmorappe 1998) and distribution of enclaves within the host rocks. As Mcbirny (2007) proposed, density reduces throughout the entire calc-alkaline series due to the steady reduction in iron and increase in silica. The calculated density by the method of Bottinga and Weill (1970) for granodioritic magmas gives an average 2392 kg/m^3.

Mineralogical evidence for magma mixing

The magma forming the Haji Abad granodiorites evolved by magma mixing, in particular mixing of mafic and felsic melts. This can be proved by the following evidence in terms of petrography and mineralogy: The widespread occurrences of ellipsoidal and spherical MMEs in the Haji Abad granodiorite with igneous microgranular textures, distinct contacts with their host rocks (Fig. 3b, f), chilled margins against the host granodiorite, and with no sign of recrystallization, deformation, and metamorphic or residual sedimentary fabrics support a magmatic origin resulting from interactions between basic and felsic magmas (e.g., Vernon 1984; Didier and Barbarin 1991; Baxter and Feely 2002; Grogan and Reavy 2002; Perugini et al. 2003; Sarjoughian et al. 2012; Yang et al. 2015) and preclude the possibility that the enclaves are fragments of recrystallized, refractory metamorphic rocks or of melt residues from the granite sources (e.g., Chappell et al. 1987, 2000; White et al. 1999), fragments of cumulates from the host magma (e.g., Noyes et al. 1983; Chen et al. 2009; Shellnutt et al. 2010; Huang et al. 2014), or xenoliths of mafic rock (e.g., Bonin 2004; Yang et al. 2004, 2006). Furthermore, the presence of K-feldspar and plagioclase megacrysts and acicular apatite in the MMEs, feldspars, and quartz that were entrained from the host granitoids to the enclaves (Fig. 3d) and the sieve texture in corroded, partially resorbed plagioclases are pieces of evidence suggesting a hybrid system formed by mixing of two distinct end-member magma compositions (e.g., Yang et al. 2015), during which the mafic magma was injected into the felsic magma and crystallization under rapid cooling in a quenched environment occurred as a result of mingling of small volumes of hot mafic melt with cooler granitoid magma (e.g., Vernon 1984; Chen et al. 2009, 2016).

Chemically oscillatory zoning in plagioclase has been widely observed in magmatic rocks (e.g., Tepley et al. 2000; Davidson et al. 2001; Halama et al. 2002; Tepley and Davidson 2003; Chen et al. 2015), especially fluctuating An and FeO contents in plagioclase that are a widespread phenomenon in subduction-related magma systems (e.g., Hattori and Sato 1996; Tepley et al. 2000; Davidson et al. 2001; Ruprecht and Wörner 2007; Andrews et al. 2008; Shcherbakov et al. 2011; Cao et al. 2014) and are an indicator to identify magmatic processes. Plagioclase crystals with oscillatory zoning in the form of anorthite fractions (Fig. 5) likely indicate the mixing of coexisting mafic and felsic magmas. Ustunisik et al. (2014) suggested that temperature, total pressure, and water content of the melts are important factors controlling compositional zoning in plagioclase, although lithospheric pressure will have a little real effect on plagioclase at a given liquid composition (Housh and Luhr 1991; Lange et al. 2009). Oxygen fugacity has obvious effects on Fe content, but not for other elements, such as partitioning of Ca between plagioclase and melt

Table 3 Representative electron microprobe analyses (wt%) and structural formulae (cpfu) of amphibole of the Haji Abad granitoids

Sample	HG45-1-A11	HG45-1-A12	HG45-1-A21	HG45-1-A22	HG45-2-A11	HG45-2-A12	HG45-2-A13	HG45-2-A21	HG45-2-A22	HG45-3-A11
SiO_2	51.31	52.06	52.50	52.56	51.04	52.51	49.58	52.33	53.10	52.16
TiO_2	0.85	0.62	0.36	0.46	0.62	0.80	0.49	0.72	0.48	0.45
Al_2O_3	3.84	3.14	3.21	3.46	4.16	3.44	3.03	3.27	3.24	3.38
FeO	9.53	9.20	9.21	9.34	10.41	8.82	8.15	9.04	8.56	9.06
MnO	0.62	0.73	0.56	0.67	0.60	0.56	0.73	0.60	0.70	0.68
MgO	17.47	18.62	18.53	18.86	17.28	17.98	15.62	18.34	18.05	18.27
CaO	11.69	11.88	11.61	11.81	11.36	11.75	10.60	11.97	11.83	11.75
Na_2O	0.74	0.66	0.58	0.68	0.71	0.66	0.70	0.70	0.61	0.66
K_2O	0.35	0.32	0.21	0.31	0.39	0.39	0.24	0.35	0.29	0.24
Cl	0.09	0.01	0.02	0.03	0.01	0.02	0.03	0.05	0.06	0.03
Cr_2O_3	0.02		0.41	0.03	0.01	0.01	8.34		0.28	0.23
Total	96.51	97.29	97.19	98.20	96.59	96.99	97.52	97.34	97.24	96.94
Si	7.327	7.330	7.365	7.309	7.260	7.434	7.096	7.385	7.490	7.364
Al^{IV}	0.646	0.521	0.530	0.566	0.698	0.566	0.512	0.543	0.510	0.563
Al^{VI}	0.000	0.000	0.000	0.000	0.000	0.008	0.000	0.000	0.028	0.000
Ti	0.092	0.066	0.038	0.048	0.067	0.085	0.053	0.077	0.051	0.048
Cr	0.003	0.000	0.045	0.003	0.001	0.001	0.944	0.000	0.031	0.025
Fe^{3+}	0.668	0.867	0.930	0.958	0.921	0.573	0.755	0.661	0.555	0.810
Fe^{2+}	0.470	0.216	0.150	0.128	0.318	0.471	0.220	0.406	0.455	0.259
Mn	0.075	0.088	0.066	0.079	0.073	0.067	0.088	0.071	0.083	0.081
Mg	3.719	3.908	3.875	3.909	3.664	3.795	3.332	3.858	3.795	3.846
Ca	1.789	1.793	1.746	1.760	1.731	1.782	1.626	1.810	1.787	1.778
Na	0.205	0.179	0.158	0.184	0.197	0.180	0.195	0.191	0.167	0.180
K	0.063	0.057	0.038	0.055	0.070	0.071	0.045	0.063	0.053	0.043
Cl	0.022	0.003	0.005	0.006	0.003	0.005	0.008	0.011	0.015	0.008
OH*	1.978	1.997	1.995	1.994	1.997	1.995	1.992	1.989	1.985	1.992
Total	17.057	17.028	16.942	17.000	16.997	17.033	16.866	17.064	17.007	17.000
Am group	Ca	Ca	Ca	Ca	Ca	Ca	Ca	Ca	Ca	Ca
(Ca+Na) (B)	2	2	2	2	2	2	2	2	2	2
Na (B)	0.205	0.179	0.158	0.184	0.197	0.180	0.195	0.190	0.167	0.180
(Na+K) (A)	0.063	0.057	0.038	0.055	0.070	0.071	0.045	0.064	0.053	0.043
$Mg/(Mg+Fe^2)$	0.888	0.948	0.963	0.968	0.920	0.890	0.938	0.905	0.893	0.937
$Fe^3/(Fe^3+Al^{VI})$	1.0	1.0	1.0	1.0	1.0	1.0	1.0	1.0	1.0	1.0

Sample	HG45-3-A12	HG45-3-A21	HG45-3-A22	HG45-6-A11	HG45-6-A12	HG45-6-A21	HG45-6-A22	HG45-7-A1	HG45-7-A2	HG45-7-A3	HG45-7-A4
SiO_2	51.89	52.19	51.92	51.06	52.05	52.10	51.50	51.03	51.61	50.52	51.50
TiO_2	0.70	0.51	0.39	0.44	0.48	0.61	0.60	0.57	0.56	0.55	0.62
Al_2O_3	3.49	3.38	3.49	3.37	2.87	3.16	3.24	3.74	3.41	3.94	3.52
FeO	8.95	9.24	9.09	9.33	8.76	8.98	9.08	9.82	9.71	9.16	9.26
MnO	0.65	0.64	0.74	0.64	0.62	0.66	0.66	0.65	0.78	0.72	0.45

Table 3 (continued)

MgO	18.13	18.60	18.00	18.35	18.56	18.43	18.30	17.76	17.67	17.65	18.35
CaO	11.79	11.78	11.63	11.88	11.65	11.55	12.05	11.84	11.28	11.69	11.77
Na_2O	0.67	0.65	0.70	0.72	0.59	0.66	0.67	0.78	0.72	0.76	0.67
K_2O	0.31	0.25	0.32	0.28	0.27	0.35	0.28	0.39	0.39	0.41	0.34
Cl	0.01	0.00	0.05	0.24	0.06	0.04	0.16	0.02	0.03	0.03	0.13
Cr_2O_3	0.06		0.02	0.04	0.53	0.25	0.05	0.02			0.01
Total	96.67	97.25	96.38	96.37	96.44	96.78	96.60	96.67	96.15	95.42	96.60
Si	7.361	7.330	7.382	7.284	7.376	7.360	7.338	7.277	7.359	7.285	7.309
Al^{IV}	0.583	0.559	0.585	0.567	0.480	0.526	0.544	0.629	0.573	0.669	0.589
Al^{VI}	0.000	0.000	0.000	0.000	0.000	0.000	0.000	0.000	0.000	0.000	0.000
Ti	0.074	0.054	0.042	0.047	0.051	0.065	0.065	0.061	0.060	0.060	0.066
Cr	0.007	0.000	0.002	0.004	0.060	0.028	0.006	0.002	0.000	0.000	0.001
Fe^{3+}	0.715	0.906	0.771	0.886	0.858	0.857	0.731	0.789	0.873	0.741	0.838
Fe^{2+}	0.347	0.179	0.309	0.227	0.180	0.203	0.350	0.382	0.285	0.363	0.261
Mn	0.078	0.077	0.089	0.078	0.074	0.079	0.080	0.079	0.094	0.088	0.054
Mg	3.833	3.895	3.816	3.904	3.921	3.881	3.886	3.775	3.756	3.793	3.883
Ca	1.792	1.772	1.772	1.815	1.769	1.748	1.839	1.809	1.723	1.806	1.790
Na	0.185	0.177	0.192	0.199	0.163	0.180	0.184	0.215	0.200	0.213	0.183
K	0.056	0.045	0.057	0.051	0.048	0.063	0.051	0.071	0.070	0.076	0.061
Cl	0.002	0.001	0.013	0.057	0.015	0.008	0.039	0.005	0.007	0.008	0.030
OH*	1.998	1.999	1.987	1.943	1.985	1.992	1.961	1.995	1.993	1.992	1.970
Total	17.033	16.994	17.021	17.065	16.980	16.991	17.075	17.096	16.993	17.094	17.034
Am group	Ca	Ca	Ca	Ca	Ca	Ca	Ca	Ca	Ca	Ca	Ca
(Ca+Na) (B)	2	2	2	2	2	1.928	2.000	2.000	1.923	2.000	1.973
Na (B)	0.185	0.177	0.192	0.185	0.163	0.180	0.161	0.191	0.200	0.194	0.183
(Na+K) (A)	0.056	0.045	0.057	0.065	0.048	0.063	0.075	0.096	0.070	0.094	0.061
$Mg/(Mg+Fe^2)$	0.917	0.956	0.925	0.945	0.956	0.950	0.917	0.908	0.930	0.913	0.937
$Fe^3/(Fe^3+Al^{VI})$	1.0	1.0	1.0	1.0	1.0	1.0	1.0	1.0	1.0	1.0	1.0

Note: Formula based on 23 oxygens

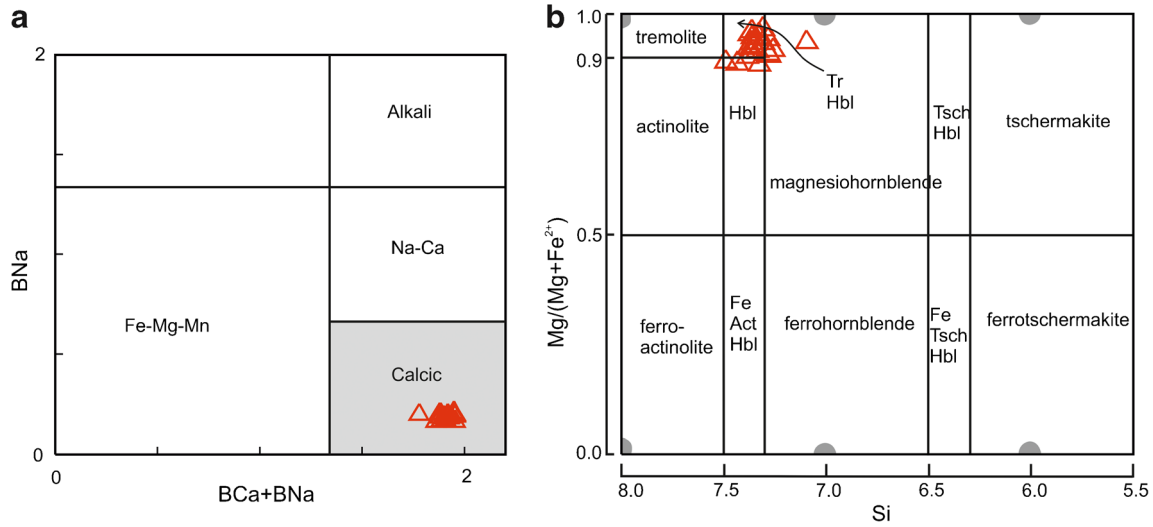

Fig. 7 **a** BCa+BNa versus BNa diagram, indicating that studied amphiboles belong to the calcic group (Leake et al. 1997). **b** Composition of amphiboles of the Haji Abad granodiorite plotted on the Si versus Mg/(Mg+Fe^{+2}) diagram (Leake et al. 1997)

(Phinney 1992; Wilke and Behrens 1999). Although An and FeO values display similar trends within the core–mantle–rim of these crystals, they do not show synchronous variations (Fig. 5). These trends indicate that oxygen fugacity variations have no important role in the observed oscillations, but these oscillations are indeed caused by changes to the melt composition, while asynchronous variations (decreasing An without decreasing FeO) suggest the effect of plagioclase crystallization which depleted Ca in the melt (Cao et al. 2014). As a result, strong correlations between An and FeO contents in plagioclase

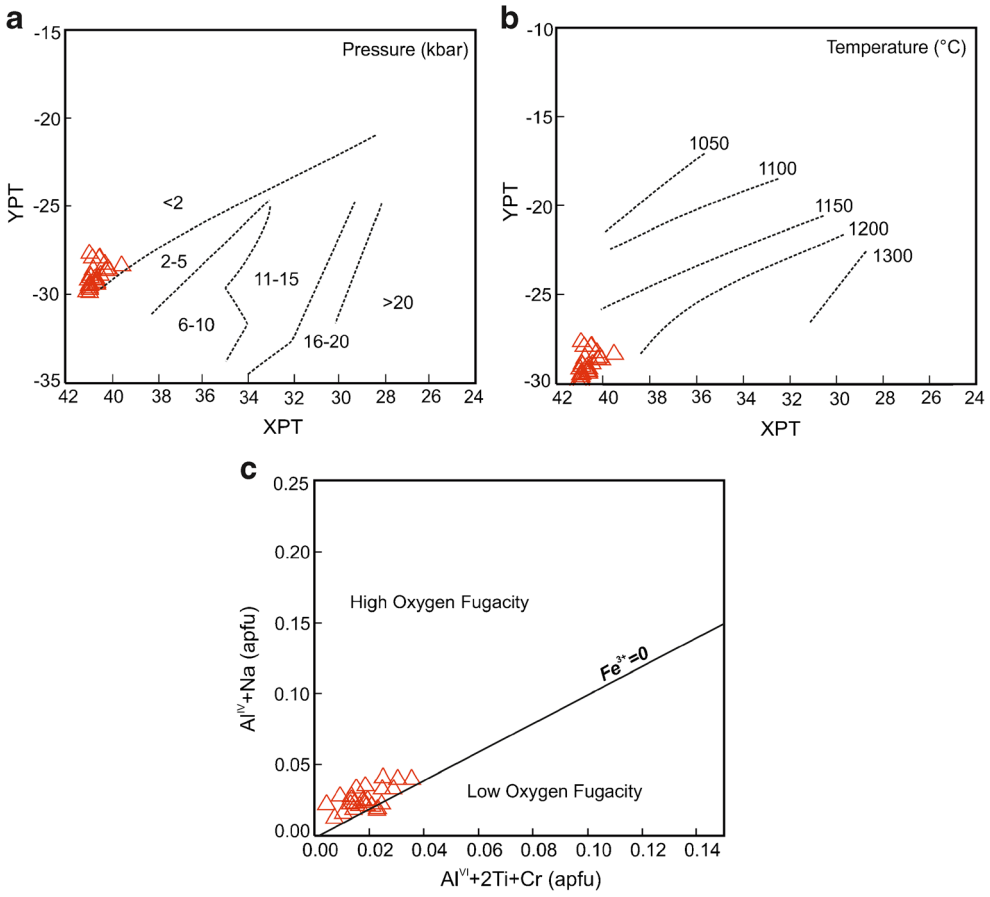

Fig. 8 **a**, **b** X_{PT} versus Y_{PT} diagrams of Soesoo (1997) for the determination of the pyroxene crystallization pressure and temperature. **c** Al^{VI}+2Ti+Cr versus Al^{IV}+Na diagram, indicating crystallization under relatively high oxygen fugacity or oxidized conditions (Schweitzer et al. 1979)

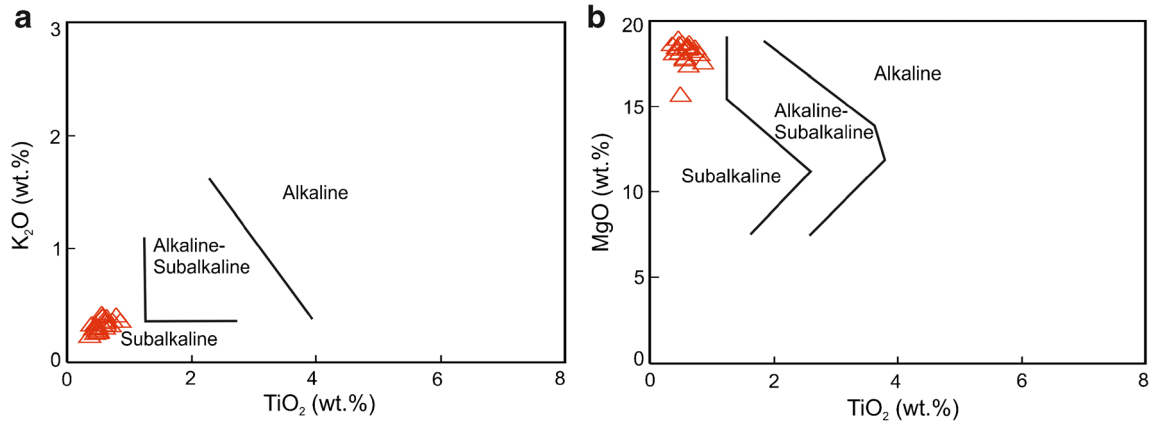

Fig. 9 **a** TiO_2 versus K_2O and **b** TiO_2 versus MgO diagrams using amphibole compositions for discrimination of geochemical affinity and tectonic environment (Molina et al. 2009)

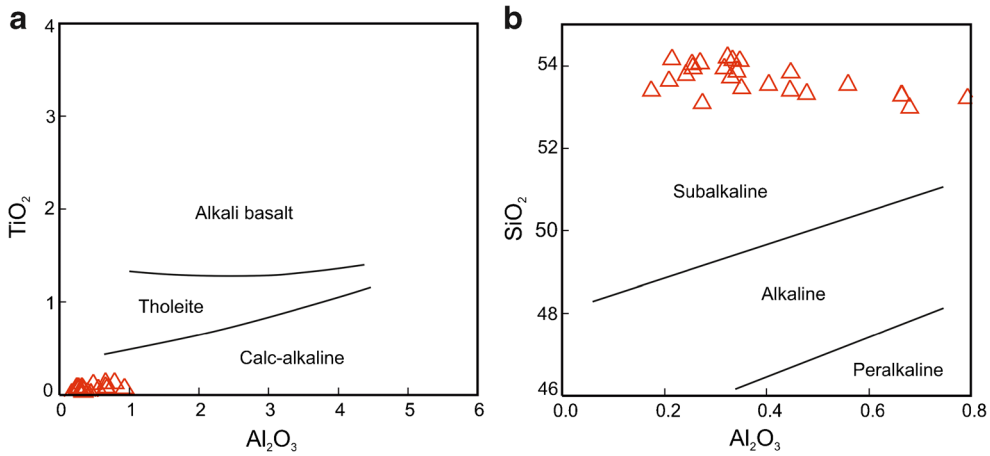

Fig. 10 **a** Al_2O_3 (wt%) versus TiO_2 (wt%) and **b** Al_2O_3 (wt%) versus SiO_2 (wt%) binary diagrams (after Le Base 1962) using composition of pyroxenes for discrimination of magmatic affinity and tectonic setting

(Fig. 5) from the Haji Abad granitoid indicate that mixing or recharging of magma took place under open-system conditions (Ruprecht and Wörner 2007). Zoned plagioclases in HAG show wide compositional oscillations from An_{10} to An_{60} and usually well-developed dissolution surfaces that can be an indicator of large-scale turbulences of the magma chamber occurring in open-system conditions, such as during magma mixing or contamination that both of them can effectively change the temperature and chemical composition (e.g., Singer et al. 1995; Hattori and Sato 1996; Davidson and Tepley 1997; Tepley et al. 1999, 2000; Davidson et al. 2001). The oscillatory patterns of chemical compositions from the core to the rim are commonly interpreted as an indicator of magma mingling in silica-intermediate rocks (Stamatelopoulou-Seymour et al. 1990).

According to the petrography and plagioclase chemistry descriptions mentioned above, it can be concluded that

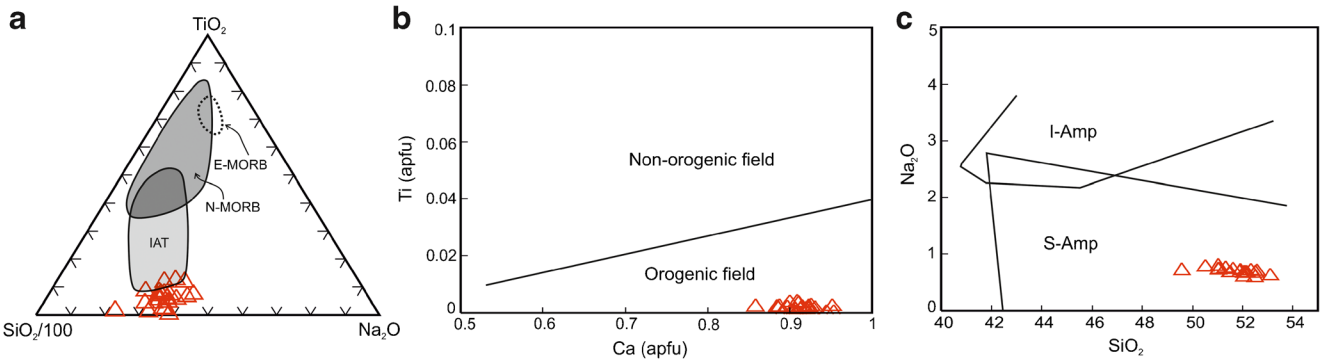

Fig. 11 **a** $SiO_2/100$–TiO_2–Na_2O ternary diagram using pyroxene composition (Beccaluva et al. 1989). **b** Plotted pyroxene data on the Ti versus Ca diagram (Sun and Bertrand 1991) fall in the orogenic field. **c** Amphiboles in Haji Abad granodiorite are plotted in the field of subduction amphibole on the Na_2O versus SiO_2 diagram (Coltorti et al. 2007)

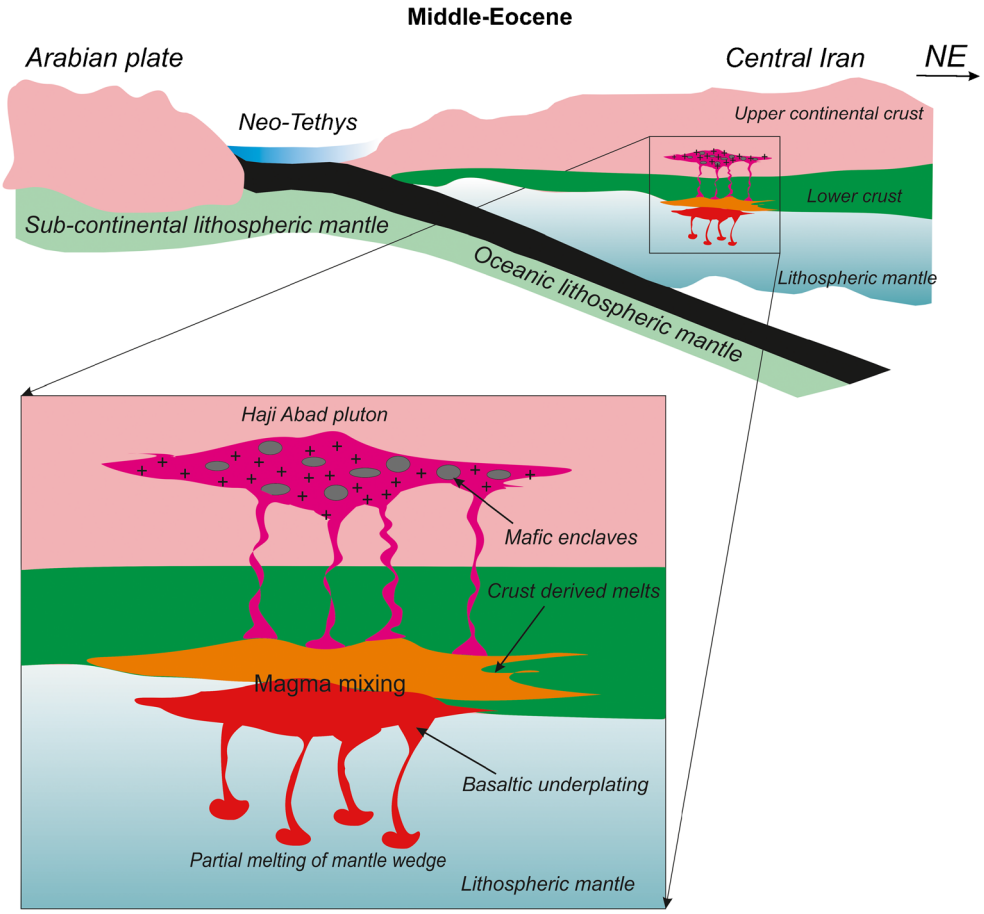

Fig. 12 Schematic model of the generation of the Haji Abad granitoids and their mafic enclaves in the UDMA during the Middle Eocene

chemical and/or thermal changes occurred in the chamber magma during crystal growth as a result of magma mixing (Baxter and Feely 2002; Grogan and Reavy 2002; Yang et al. 2015).

Nature of magma and tectonic environment

The mineral chemistry of ferromagnesian minerals (such as pyroxene, amphibole, and biotite) is a function of chemical composition and tectonic setting of their formative magma and can provide valuable information about tectonic setting and petrogenesis of the granitoid rocks (Maulana et al. 2012). According to many researchers (Chappel and White 1974; Wyborn et al. 1981; White and Chappell 1983; Clemens and Wall 1984), the presence of calcic amphiboles in granitoid rocks indicates that these rocks belong to the I-type granitoids (Stein and Dietl 2001), because the abundance of CaO in these granites leads to hornblende crystallization.

Molina et al. (2009) suggested that the incorporation of K, Mg, and Ti into the amphibole structure depends of the nature of magma, as the amphiboles in the subalkaline series have lower TiO_2 (< 2 wt%) and K_2O than those found in alkaline series. According to Molina et al. (2009), on the TiO_2 versus K_2O and TiO_2 versus MgO discrimination diagrams (Fig. 9), the studied amphiboles are grouped in the subalkaline fields that are consistent with crystallization from I-type calc-alkaline magma in a subduction environment related to active continental margin. Clinopyroxene compositions, especially element contents such as Ti, Al, Na, Cr, and Si, can be used to identify the magmatic affinity and geotectonic environment (e.g., Le Base 1962; Leterrier et al. 1982; Sun and Bertrand 1991). Le Base 1962 has believed that it is possible to separate peralkaline, alkaline, and subalkaline magmatic series using the SiO_2, Al_2O_3, and TiO_2 contents in the chemical composition of pyroxene. Pyroxene in granodiorites is rich in Si and poor in Ti and Al and, in the SiO_2 and TiO_2 versus Al_2O_3 diagrams (Fig. 10), plots in the fields of subalkaline and calc-alkaline, respectively. The above results are in agreement with geochemical data (Tabbakh Shabani 1991; Safarzadeh et al. 2007; Kazemi et al. 2018). As Kazemi et al. (2018) suggested, these rocks are metaluminous and calc-alkaline in character with low A/CNK (molar $Al_2O_3/(CaO+Na_2O+K_2O)$) ratios from 0.69 to 1.03 and A/NK (molar Al_2O_3/Na_2O+K_2O) ratios from 1.37 to 2.54, indicative of an I-type affinity for these rocks.

The frequency of elements such as Al, Ti, Cr, Na, and especially Si in the chemical composition of pyroxene is an indicator of their nature and tectonic setting (Le Base 1962;

Leterrier et al. 1982; Sun and Bertrand 1991). As shown in Fig. 11a, low contents of Ti and high SiO_2 contents in the studied pyroxene structure are characteristic of arc volcanic igneous rocks (Beccaluva et al. 1989). Furthermore, the plotted pyroxene data on the Ti versus Ca diagram (Sun and Bertrand 1991) indicates that the HAG rocks were generated in an orogenic belt (Fig. 11b). The studied amphiboles have low contents of Na_2O and TiO_2. Coltorti et al. (2007) proposed that suprasubduction amphiboles (S-Amph) generally show lower contents of Na_2O and TiO_2 than intraplate amphiboles (I-Amph). Also, amphiboles in Haji Abad granodiorite are plotted in the field of subduction amphibole on the Na_2O versus SiO_2 diagram (Fig. 11c; Coltorti et al. 2007). As shown in Fig. 10, the low content of Ti and the high content of SiO_2 in the pyroxene structure indicate the characteristics of pyroxenes in igneous rocks associated with volcanic arc (Beccaluva et al. 1989). A subduction zone setting for the studied intrusion is also supported by geochemical data (Tabbakh Shabani 1991; Safarzadeh et al. 2007; Kazemi et al. 2018). Many researchers proposed the Neo-Tethyan subduction beneath central Iran as the interpretation of the origin of magmatism in the UDMA (Rezaei-Kahkhaei et al. 2011; Honarmand et al. 2012; Sarjoughian et al. 2012; Kananian et al. 2014; Sarjoughian et al. 2018). For instance, Honarmand et al. (2012) using clinopyroxene and biotite composition suggested that Natanz pluton formed from a calc-alkaline magma in a subduction zone setting. Also, Sarjoughian et al. (2018) based on geochemical data proposed that Zafarghand igneous complex in the UDMA formed in an active continental margin setting, which was emplaced during subduction of Neo-Tethyan oceanic crust beneath the Sanandaj–Sirjan and central Iran zones. Consequently, the HAG represents an orogenic cycle, and the mixing processes possibly took place in an active continental margin during northeastward subduction of Neo-Tethyan oceanic crust underneath the central Iranian microcontinent (Fig. 12).

Conclusions

1. The Haji Abad intrusion is a well-exposed I-type granodioritc pluton in the central part of the UDMA. Two-feldspar and clinopyroxene thermometers yield crystallization temperatures with an average of 724 and 1090 °C. The calculated pyroxene and feldspar temperatures represent the first and late stages of magmatic crystallization of Haji Abad granodiorite, respectively.
2. Meanwhile, the calculated average pressures of emplacement are 1.9 kbar for the granodioritic rocks, which is equal to depths of about 6.7 km based on the two barometer equations of clinopyroxene. The highest calculated pressure (5 kbar) reflects initial pyroxene crystallization pressure, indicating initial crystallization depth (17.5 km) in the Haji Abad granodiorite.
3. The oxygen fugacity estimates according to pyroxene are above the line of $Fe^{3+} = 0$, indicating that the Haji Abad magmas were characterized by relatively high oxygen fugacity or oxidized conditions. Furthermore, the results show that the rocks crystallized from magmas with H_2O content of 3.2 wt%. The calculated water content is consistent with the generation environment of HAG rocks in active continental margins.
4. The widespread ellipsoidal and spherical MMEs with igneous micogranular textures and chilled margins in the Haji Abad granodiorite; the presence of K-feldspar and plagioclase megacrysts and acicular apatite in the MMEs, feldspars, and quartz that were entrained from the host granitoids to the enclaves; and sieve texture in corroded, partially resorbed plagioclases, together with An and FeO oscillatory patterns in the plagioclase, suggest a hybrid system formed by mixing of two distinct end-member magma compositions, during which the mafic magma was injected into the felsic magma, and crystallization under rapid cooling in a quenched environment occurred as a result of mixing/mingling of hot mafic melt with cooler granitoid magma, since chemical and/or thermal changes occurred in the chamber magma during crystal growth as a result of magma mixing.
5. The studied amphiboles and pyroxenes are grouped in the subalkaline fields that are consistent with crystallization from I-type calc-alkaline magma in a subduction environment related to active continental margin, indicating the generation of HAG in an orogenic belt related to the volcanic arc setting consistent with the subduction of Neo-Tethyan oceanic crust beneath the central Iranian microcontinent.

Acknowledgements This study is a synthesis of the Ph.D. thesis by K. Kazemi. The authors acknowledge the support of this project by the University of Tehran. The electron probe microanalyses (EPMA) of mineral were carried out at the Hefei University, China. We would like to thank Dr. Hou Zhenhui, Mr. Yangyang Wang, and Mr. Fengtai Tong for their help during sabbatical at USTC and for their technical assistance. This work is partly supported by projects from the National Natural Science Foundation of China (41473033, 41673031).

References

Abbasi S, Tabatabaei Manesha SM, Karimia S, Parfenova OV (2014) Relative contributions of crust and mantle to generation of Oligo–Miocene medium-K calc-alkaline I-type granitoids in a subduction setting—a case study from the Nabar pluton, central Iran. Petrology 22:310–328

Abbott RN Jr (1985) Muscovite-bearing granites in the AFM liquidus projection. Can Mineral 23:553–561

Aghanabati A (1998) Major sedimentary and structural units of Iran (map). Geosciences 7, Geological Survey of Iran

Alavi M (2004) Regional stratigraphy of the Zagros Fold-Thrust Belt of Iran and its proforeland evolution. Am J Sci 304:1–20

Allen MB (2009) Discussion on the Eocene bimodal Piranshahr massif of the Sanandaj–Sirjan zone, west Iran: a marker of the end of collision in the Zagros orogen. J Geol Soc London 166:981–982

Anderson AT Jr (1980) Significance of hornblende in calc-alkaline andesites and basalts. Am Mineral 65:837–851

Anderson JL (1996) Status of thermo-barometry in granitic batholiths. Earth Sci Rev 87:125–138

Andrews BJ, Gardner JE, Housh TB (2008) Repeated recharge, assimilation, and hybridization in magmas erupted from El Chichón as recorded by plagioclase and amphibole phenocrysts. J Volcanol Geotherm Res 175:415–426

Arvin M, Pan Y, Dargahi S, Malekizadeh A, Babaei A (2007) Petrochemistry of the Siah Kuh granitoid stock southwest of Kerman, Iran: implications for initiation of Neotethys subduction. J Asian Earth Sci 30:474–489

Ayati F, Yavuz F, Asadi HH, Richards JP, Jourdan F (2013) Petrology and geochemistry of calc-alkaline volcanic and subvolcanic rocks, Dalli porphyry copper-gold deposit, Markazi Province, Iran. Int Geol Rev 55:158–184

Barbarin B (2005) Mafic magmatic enclaves and mafic rocks associated with some granitoids of the Central Sierra Nevada batholiths, California: nature, origin, and relations with the hosts. Lithos 80: 155–177

Baxter S, Feely M (2002) Magma mixing and mingling textures in granitoids: examples from the Galway granite, Connemara, Ireland. Mineralogy and Petrology 76:63–74

Beccaluva L, Macciotta G, Piccardo GB, Zeda O (1989) Clinopyroxene composition of ophiolite basalts as petrogenetic indicator. Chem Geol 77:165–182

Berberian F, Berberian M (1981) Tectono-plutonic episodes in Iran. In: Gupta HK, Delany FM (eds) Zagroz Hindu Kush Himalaya geodynamic evolution. American Geophysical Union & Geological Society of America, Washington, pp 5–32

Berberian M, King GCP (1981) Towards a paleogeography and tectonic evolution of Iran. Can J Earth Sci 18:210–265

Bonin B (2004) Do coeval mafic and felsic magmas in post-collisional to within-plate regimes necessarily imply two constrasting, mantle and crust, sources? A review. Lithos 78:1–24

Botcharnikov R, Koepke J, Holtz F, McCammon C, Wilke M (2005) The effect of water activity on the oxidation and structural state of Fe in a ferro-basaltic melt. Geochim Cosmochim Acta 69:5071–5085

Bottinga Y, Weill DF (1970) Densities of liquid silicate systems calculated from partial molar volumes of oxide components. Am J Sci 269: 169–182

Caillat C, Dehlavi P, Martel-Jantin B (1978) Géologie de la région de Saveh (Iran); contribution à l'étude du volcanisme et du plutonisme tertiaires de la zone de l'Iran Central. Thèse de Doctorat de Specialities, Grenoble University, France 325 pp.

Cao M, Qin K, Li J, Yang Y, Evans NJ, Zhang R, Jin L (2014) Magmatic process recorded in plagioclase at the Baogutu reduced porphyry Cu deposit, western Junggar, NW-China. J Asian Earth Sci 82:136–150

Chappel BW, White AJR (1974) Two contrasting granite types. Pacific Geology 8:173–174

Chappell BW, White AJR, Williams IS, Wyborn D, Wyborn LAI (2000) Lachlan Fold Belt granites revisited: high- and low-temperature granites and their implications. Aust J Earth Sci 47:123–138

Chappell BW, White AJR, Wyborn D (1987) The importance of residual source material (restite) in granite petrogenesis. J Petrol 28:1111–1138

Chen B, Chen ZC, Jahn BM (2009) Origin of the mafic enclaves from the Taihang Mesozoic orogen, North China craton. Lithos 110:343–358

Chen CJ, Chen B, Li Z, Wang ZQ (2016) Important role of magma mixing in generating the Mesozoic monzodioritic–granodioritic intrusions related to Cu mineralization, Tongling, East China: evidence from petrological and in situ Sr-Hf isotopic data. Lithos 248–251:80–93

Chen WT, Zhou MF, Gao JF, Zhao TP (2015) Oscillatory Sr isotopic signature in plagioclase megacrysts from the Damiao anorthosite complex, North China: implication for petrogenesis of massif-type anorthosite. Chem Geol 393–394:1–15

Claeson DT, Meurer WP (2004) Fractional crystallization of hydrous basaltic "arctype" magmas and the formation of amphibole-bearing gabbroic cumulates. Contrib Mineral Petrol 147:288–304

Clarke DB (1992) Granitoid rocks. Chapman and Hall, London

Clemens JD, Wall VJ (1984) Origin and evolution of a peraluminous silicic ignimbrite suite: the Violet Town Volcanics. Contrib Mineral Petrol 88:354–371

Coltorti M, Bondaiman C, Faccini B, Gregoire M, OReilly SY, Powell W (2007) Amphiboles from suprasubduction and intraplate lithospheric mantle. Lithos 99:68–84

Davidson J, Turner S, Handley H, Macpherson C, Dosseto A (2007) Amphibole "sponge" in arc crust. Geology 35:787–790

Davidson JP, Tepley F III, Palacz Z, Meffan-Main S (2001) Magma recharge, contamination and residence times revealed by in situ laser ablation isotopic analysis of feldspar in volcanic rocks. Earth Planet Sci Lett 184:427–442

Davidson JP, Tepley FJ (1997) Recharge in volcanic systems: evidence from isotope profiles of phenocrysts. Science 275:826–829

Deer WA, Howie RA, Zussman J (1992) An introduction to the rock-forming minerals. Longman, Essex

Dessimoz M, Müntener O, Ulmer P (2012) A case for hornblende dominated fractionation of arc magmas: the Chelan complex (Washington cascades). Contrib Mineral Petrol 163:567–589

Didier J, Barbarin B (1991) Enclaves and granite petrology. Elsevier, Amsterdam, pp 1–626

Dorouzi T, Vosoughi Abedini M (2009) The role of magmatic fractionation and crustal contamination in the genesis of south and south eastern Buin-Zahra Eocene volcanic rocks. Iran J Geol 3:15–23 (In Persian with English abstract)

Eghlimi B (2000) Geological map of Danesphahan 1:100000 survey sheet. Geological Survey of Iran

Elkins LT, Grove TL (1990) Ternary feldspar experiments and thermodynamic models. Am Mineral 75:544–559

Ernst WG (1999) Hornblende, the continental maker—evolution of H_2O during circumPacific subduction versus continental collision. Geology 27:675–678

Faak K, Chakraborty S, Coogan LA (2013) Mg in plagioclase: experimental calibration of a new geothermometer and diffusion coefficients. Geochim Cosmochim Acta 123:195–217

Förster H, Fesefeldt K, Kürsten M (1972) Magmatic and orogenic evolution of the central Iranian volcanic belt. In: Armstrong JE, Hedberg HD (eds.) 24th international geologic congress, Montreal, QC, Canada 198–210

France L, Koepke J, Ildefonse B, Cichy SB, Deschamps F (2010) Hydrous partial melting in the sheeted dike complex at fast spreading ridges: experimental and natural observations. Contrib Mineral Petrol 160:683–704

Fuhrman ML, Lindsley DH (1988) Ternary-feldspar modeling and thermometry. Am Mineral 73:201–215

Grogan SE, Reavy RJ (2002) Disequilibrium textures in the Leinster granite complex, SE Ireland: evidence for acid-acid magma mixing. Mineral Mag 66:929–939

Halama R, Waight T, Markl G (2002) Geochemical and isotopic zoning patterns of plagioclase megacrysts in gabbroic dykes from the Gardar Province, South Greenland: implications for crystallization processes in anorthositic magmas. Contrib Mineral Petrol 144:109–127

Hammarstrom JM, Zen E (1986) Aluminum in hornblende: an empirical igneous geobarometer. Am Mineral 71:1297–1313

Hattori K, Sato H (1996) Magma evolution recorded in plagioclase zoning in 1991 Pinatubo eruption products. Am Mineral 81:982–994

Helz RT (1973) Phase relations of basalts in their melting range at PH_2O=5 kb as a function of oxygen fugacity, part I: mafic phases. J Petrol 14:249–302

Honarmand M, Ahmadian J, Nabatian G, Murata M (2012) Reconstructing physicochemical conditions by application of mineral chemistry: a case study from the Natanz pluton, Central Iran. Neues Jahrbuch fur Mineralogie, Abhandlungen 189:138–153

Honarmand M, Rashidnejad Omran N, Neubauer F, Nabatian G, Emami MH, Bernroider M, Ahmadian J, Ebrahimi M, Liu X (2016) Mineral chemistry of a Cenozoic igneous complex, the Urumieh–Dokhtar magmatic belt, Iran: petrological implications for the plutonic rocks. Island Arc 25:137–153

Housh TB, Luhr JF (1991) Plagioclase-melt equilibria in hydrous systems. Am Mineral 76:477–492

Huang H, Niu YL, Nowell G, Zhao ZD, Yu XH, Zhu DC, Mo XX, Ding S (2014) Geochemical constraints on the petrogenesis of granitoids in the east Kunlun orogenic belt, northern Tibetan plateau: implications for continental crust growth through syn-collisional felsic magmatism. Chem Geol 370:1–18

Kananian A, Sarjoughian F, Nadimi A, Ahmadian J, Ling W (2014) Geochemical characteristics of the Kuh-e Dom intrusion, Urumieh Dokhtar Magmatic Arc (Iran): implications for source regions and magmatic evolution. J Asian Earth Sci 90:137–148

Kazemi K, Kananian A, Xiao Y, Sarjoughian F (2018) Petrogenesis of Middle-Eocene granitoids and their mafic microgranular enclaves in central Urmia-Dokhtar Magmatic Arc (Iran): evidence for interaction between felsic and mafic magmas. Geosci Front. https://doi.org/10.1016/j.gsf.2018.04.006

Krawczynski MJ, Grove TL, Behren H (2012) Amphibole stability in primitive arc magmas: effects of temperature, H_2O content, and oxygen fugacity. Contrib Mineral Petrol 164:317–339

Kretz R (1983) Symbols for rock-forming minerals. Am Mineral 68:277–279

Kudo AM, Weill DF (1970) An igneous plagioclase thermometer. Contrib Mineral Petrol 25:52–65

Lange RA, Frey HM, Hector J (2009) A thermodynamic model for the plagioclase liquid hygrometer/thermometer. Am Mineral 94:494–506

Larocque J, Canil D (2010) The role of amphibole in the evolution of arc magmas and crust: the case from the Jurassic Bonanza arc section, Vancouver Island, Canada. Contrib Mineral Petrol 159:475–492

Le Base MJ (1962) The role of aluminum in igneous clinopyroxenes with relation to their parentage. Am J Sci 260:267–288

Leake BE, Woolly AR, Arps CES, Birch WD, Gilbert MC, Grice JD, Hawthorne FC, Kato A, Kisch HJ, Krivovichev VG et al (1997) Nomenclature of amphiboles. Report of the Subcommittee on Amphiboles of the International Mineralogical Association Commission on New Minerals Names. Eur J Mineral 9:623–651

Leterrier J, Maury RC, Thonon P, Girard D, Marchal M (1982) Clinopyroxene composition as a method of identification of the magmatic affinities of paleo-volcanic series. Earth Planet Sci Lett 59:139–154

Martin RF (2007) Amphiboles in the igneous environment, in: Hawthorne FC, Oberti R (Eds.), Amphiboles: crystal chemistry, occurrence and human health. Reviews in mineralogy and geochemistry 67:323–358

Maulana A, Watanabe K, Imai A, Yonezu K (2012) Geochemical signature of granitic rocks from Sulawesi, Indonesia: evidence of Gondwana involvement. Mineralogical Magazine 76:2081pp

Mcbirny AR (2007) Igneous petrology, third edn. Jones and Bartlett, Boston

Moine-Vaziri H (1985) Volcanisme tertiarie et quaternaire en Iran: These d Etat. Univers. Paris-Sud, Orsay

Molina J, Scarrow J, Montero PG, Bea F (2009) High-Ti amphibole as a petrogenetic indicator of magma chemistry: evidence for mildly alkalic-hybrid melts during evolution of Variscan basic–ultrabasic magmatism of Central Iberia. Contrib Mineral Petrol 158:69–98

Morimoto N, Fabries J, Ferguson AK, Ginzburg IV, Ross M, Seifert FA, Zussman J, Aoki K, Gottardi D (1988) Nomenclature of pyroxenes. Am Mineral 62:53–62

Morimoto N, Fabries J, Ferguson AK, Ginzburg IV, Ross M, Seifert FA, Zussman J, Aoki K, Gottardi G (1989) Nomenclature of pyroxenes. Subcommittee on pyroxenes. Am Mineral 73:1123–1133

Morley CK, Kongwung B, Julapour AA, Abdolghafourian M, Hajian M, Waples D, Warren J, Otterdoom H, Srisuriyon K, Kazemi H (2009) Structural development of a major late Cenozoic basin and transpressional belt in central Iran: the Central Basin in the Qom-Saveh area. Geosphere 5:325–362

Murphy JB, Blais SA, Tubrett M, McNeil D, Middleton M (2012) Microchemistry of amphiboles near the roof of a mafic magma chamber: insights into high level melt evolution. Lithos 148:162–175

Nekvasil H, Burnham CW (1987) The calculated individual effects of pressure and water content on phase equilibria in the granites system. In: Mysen BO (eds) Magmatic process: physicochemical principles. Geochemical Society, University Park, Pennsylvania. 500 p

Nogole-Sadat MAA, Hoshmandzadeh A (1984) Saveh geological map, scale 1:250000, Geological Survey of Iran

Noyes H, Frey FA, Wones DR (1983) A tale of two plutons: geochemical evidence bearing on the origin and differentiation of the Red Lake and Eagle Peak plutons, central Sierra Nevada, California. J Geol 91:487–509

Panjasawatwong Y, Danyushevsky LV, Crawford AJ, Harris KL (1995) An experimental study of the effects of melt composition on plagioclase-melt equilibria at 5 and 10 kbar: implications for the origin of magmatic high-An plagioclase. Contrib Mineral Petrol 118:420–432

Papike JJ, Cameron M (1976) Crystal chemistry of silicate minerals of geophysical interest. Rev Geophys 14:37–80

Perugini D, Poli G, Christofides G, Eleftheriadis G (2003) Magma mixing in the Sithonia Plutonic Complex, Greece: evidence from mafic microgranular enclaves. Mineral Petrol 78:173–200

Phinney WC (1992) Partition coefficients for iron between plagioclase and basalt as a function of oxygen fugacity: implications for Archean and lunar anorthosites. Geochim Cosmochim Acta 56:1885–1895

Putirka KD (2005) Igneous thermometers and barometers based on plagioclase + liquid equilibria: tests of some existing models and new calibrations. Am Mineral 90:336–346

Putirka KD (2008) Thermometers and barometers for volcanic systems. Rev Mineral Geochem 69:61–120

Putirka KD, Mikaelian H, Ryerson F, Shaw H (2003) New clinopyroxene-liquid thermobarometers for mafic, evolved, and volatile-bearing lava compositions, with applications to lavas from Tibet and the Snake River Plain, Idaho. Am Mineral 88:1542–1554

Rezaei-Kahkhaei M, Galindo G, Pankhurst RJ, Esmaeily D (2011) Magmatic differentiation in the calc-alkaline Khalkhab Neshveh pluton, Central Iran. J Asian Earth Sci 42:499–514

Ridolfi F, Renzulli A, Puerini M (2010) Stability and chemical equilibrium of amphibole in calc-alkaline magmas: an overview, new thermobarometric formulations and application to subduction-related volcanoes. Contrib Mineral Petrol 160:45–66

Ruprecht P, Wörner G (2007) Variable regimes in magma systems documented in plagioclase zoning patterns: El Misti stratovolcano and Andahua monogenetic cones. J Volcanol Geotherm Res 165:142–162

Rutter MJ, Van der laan SR, Wyllie PJ (1989) Experimental data for a proposed empirical igneous geobarometer: aluminium in hornblende at 10 kbar pressure. Geology 17:897–900

Safarzadeh E, Vosoughi Abedini M, Ghorbani M (2007) Nature and source of Haji Abad granitoidic pluton. 11th symposium of Geological Society of Iran, Ferdowsi University of Mashahd, Iran (In Persian with English abstract)

Sarjoughian F (2012) Nature of the Kuh-e Dom plutonism (NE Ardestan), geological events and its magmatic evolution. Ph.D thesis, University of Tehran, Tehran (In Persian with English abstract)

Sarjoughian F, Kananian A, Haschke M, Ahmadian J, Ling W (2012) Magma mingling and hybridization in the Kuh-e Dom pluton, Central Iran. J Asian Earth Sci 54-55:49–63

Sarjoughian F, Kananian A, Lentz DR, Ahmadian J (2015) Nature and physicochemical conditions of crystallization in the South Dehgolan intrusion, NW Iran: mineral-chemical evidence. Turk J Earth Sci 24: 249–275

Sarjoughian F, Lentz D, Kananian A, Ao S, Xiao W (2018) Geochemical and isotopic constraints on the role of juvenile crust and magma mixing in the UDMA magmatism, Iran: evidence from mafic microgranular enclaves and cogenetic granitoids in the Zafarghand igneous complex. Int J Earth Sci 107(3):1127–1151

Schmidt MW (1992) Amphibole composition in tonalite as a function of pressure an experimental calibration of the Alhornblende barometer. Contrib Mineral Petr 110:304–310

Schweitzer EL, Papike JJ, bence AE (1979) Statitical analysis of clinopyroxenes from deep sea basalts. Am Mineral 64:501–513

Sepahi AA, Maanijou M, Salami S et al (2012) Mineral chemistry and geothermobarometry of Moshirabad pluton, Qorveh, Kurdistan, western Iran. Island Arc 21(3):170–187

Shcherbakov V, Plechov P, Izbekov P, Shipman J (2011) Plagioclase zoning as an indicator of magma processes at Bezymianny volcano, Kamchatka. Contrib Mineral Petrol 162:83–99

Shelley D (1993) Igneous and metamorphic rocks under the microscope. Chapman and Hall, London

Shellnutt JG, Jahn BM, Dostal J (2010) Elemental and Sr–Nd isotope geochemistry of microgranular enclaves from peralkaline A-type granitic plutons of the Emeishan large igneous province, SW China. Lithos 19:34–46

Sherafat S, Yavuz F, Noorbehesht I, Yıldırım DK (2012) Mineral chemistry of Plio-Quaternary subvolcanic rocks, Southwest Yazd Province, Iran. Int Geol Rev 54(13):1497–1531

Singer BS, Dungan M, Layne GD (1995) Textures and Sr, Ba, Mg, Fe, K, and Ti compositional profiles in volcanic plagioclase: clues to the dynamics of calcalkaline magma chambers. Am Mineral 80:776–798

Snelling AA, Woodmorappe J (1998) In: The cooling of thick igneous bodies on a young earth. Fourth international conference on creationism, Pittsburgh, Pennsylvania, August 527–545

Soesoo A (1997) A multivariate statistical analysis of clinopyroxene composition: empirical coordinates for the crystallisation PT-estimations. Geol Soc Sweden (Geologiska Föreningen) 119:55–60

Stamatelopoulou-Seymour K, Vlassopoulos D, Pearce TH, Rice C (1990) The record of magma chamber processes in plagioclase phenocrysts at Thera Volcano, Aegean Volcanic Arc, Greece. Contrib Mineral Petrol 104:73–84

Stein E, Dietl E (2001) Hornblende thermobarometry of granitoids from the central Odenwald (Germany) and their implication for the geotectonic development of the Odenwald. Mineral Petrol 72:185–207

Sun CM, Bertrand J (1991) Geochemistry of clinopyroxenes in plutonic and volcanic sequences from the Yanbian Proterozoic ophiolites (Sichuan Province, China): petrogenetic and geotectonic implications. Schweiz Mineralogische Petrologische Mitteilungen 71:243–259

Tabbakh Shabani A (1991) Petrogeraphy and petrology of Boin zahra igneouse intrusive bodies, M.S. thesis, Tarbiat Moalem University, Tehran (In Persian with English abstract)

Tepley FJ III, Davidson JP (2003) Mineral-scale Sr-isotope constraints on magma evolution and chamber dynamics in the rum layered intrusion, Scotland. Mineral Petrol 145:628–641

Tepley FJ III, Davidson JP, Tilling RI, Arth JG (2000) Magma mixing, recharge and eruption histories recorded in plagioclase phenocrysts from El Chichon volcano, Mexico. J Petrol 41:1397–1411

Tepley FJ, Davidson JP, Clynne MA (1999) Magmatic interactions as recorded in plagioclase phenocrysts of Chaos Crags, Lassen Volcanic Center, California. J Petrol 40:787–806

Tulloch AJ, Challis GA (2000) Emplacement depths of Paleozoic-Mesozoic plutons from western New Zealand estimated by hornblende-Al geobarometry. N Z J Geol Geophys 43:555–567

Ustunisik G, Kilinc A, Nielsen RL (2014) New insights into the processes controlling compositional zoning in plagioclase. Lithos 200/201: 80–93

Vernon RH (1984) Microgranitoid enclaves in granites-globules of hybrid magma quenched in a plutonic environment. Nature 309:438–439

Vernon RH (1990) Crystallization and hybridism in microgranitoid enclave magmas: microstructural evidence. J Geophys Res 95:17849–17859

Vyhnal CR, McSween HY Jr, Speer JA (1991) Hornblende chemistry in southern Appalachian granitoids: implications for aluminum hornblende thermobarometry and magmatic epidote stability. Am Mineral 76:176–188

White AJR, Chappell BW (1983) Granitoid types and their distribution in the Lachlan Fold Belt, southeastern Australia. Geol Soc Am Memory 159:21–34

White AJR, Chappell BW, Wyborn D (1999) Application of the restite model to the Deddick granodiorite and its enclaves—a reinterpretation of the observations and data of Maas et al (1997). J Petrol 40: 413–421

Wilke M, Behrens H (1999) The dependence of the partitioning of iron and europium between plagioclase and hydrous tonalitic melt on oxygen fugacity. Contrib Mineral Petrol 137:102–114

Wyborn D, Chappell BW, Johnston RM (1981) Three S type volcanic suites from the Lachlan Fold Belt, Southeast Australia. J Geophys Res 86:10335–10348

Yang H, Ge W, Zhao G, Dong Y, Xu WL, Ji Z, Yu J (2015) Late Triassic intrusive complex in the Jidong region, Jiamusi–Khanka block, NE China: geochemistry, zircon U–Pb ages, Lu–Hf isotopes, and implications for magma mingling and mixing. Lithos 224-225:143–159

Yang JH, Wu FY, Chung SL, Wilde SA, Chu MF (2004) Multiple sources for the origin of granites: geochemical and Nd/Sr isotopic evidence from the Gudaoling granite and its mafic enclaves, NE China. Geochim Cosmochim Acta 68:4469–4483

Yang JH, Wu FY, Chung SL, Wilde SA, Chu MF (2006) A hybrid origin for the Qianshan A-type granite, northeast China: geochemical and Sr–Nd–Hf isotopic evidence. Lithos 89:89–106

Zhang SH, Zhao Y, Song B (2006) Hornblende thermobarometry of the carboniferous granitoids from the Inner Mongolia paleo-uplift: implications for the tectonic evolution of the northern margin of North China block. Mineral Petrol 87:123–141

Zorpi MJ, Coulon C, Orisini JB, Concirta C (1989) Magma mingling, zoning and emplacement in calk-alkaline granitoid plutons. Tectonophysics 157:315–326